

## Geospatial approach towards enumerative analysis of Suspended Sediment Concentration for Ganges-Brahmaputra Bay

**Palak Pandey<sup>a</sup> and Pravin D. Kunte<sup>\*b</sup>**

<sup>a</sup>Geo-Informatics, University of Petroleum and Energy Studies, Dehradun

<sup>\*b</sup>CSIR-National Institute of Oceanography, Dona Paula-403004, Goa, India. [kunte@nio.org](mailto:kunte@nio.org)

### **ABSTRACT**

This study presents an easy, modular, user-friendly, and flexible software package for processing of Landsat 7 ETM and Landsat 8 OLI-TIRS data for estimating suspended particulate matter concentrations in the coastal waters. This package includes 1) algorithm developed using freely downloadable SCILAB package, 2) ERDAS Models for iterative processing of Landsat images and 3) ArcMAP tool for plotting and map making. Utilizing SCILAB package, a module is written for geometric corrections, radiometric corrections and obtaining normalized water-leaving reflectance by incorporating Landsat 8 OLI-TIRS and Landsat 7 ETM+ data. Using ERDAS models, a sequence of modules are developed for iterative processing of Landsat images and estimating suspended particulate matter concentrations. Processed images are used for preparing suspended sediment concentration maps. The applicability of this software package is demonstrated by estimating and plotting seasonal suspended sediment concentration maps off the Bengal delta. The software is flexible enough to accommodate other remotely sensed data like Ocean Color monitor (OCM) data, Indian Remote Sensing data (IRS), MODIS data etc. by replacing a few parameters in the algorithm, for estimating suspended sediment concentration in coastal waters.

## 1. INTRODUCTION

Estimating suspended particulate matter concentrations (SPM) over long coastal areas using customary way of in-situ sampling is a lengthy, costly, and laborious process. In contrast, remotely detected spectral radiant energy estimated by satellite sensors can deliver a different, synoptic, rapid, and economical approach for assessing the SPCs in coastal water bodies, lakes, and rivers (McKim *et al.*, 1984; Curran and Wilkinson, 1985). However, effective algorithms are essential for converting radiance or reflectance values into measurement of water constituents. In sediment-dominated coastal waters, sophisticated algorithms are mainly needed to estimate accurately the suspended particulate concentrations from remotely sensed ocean color data (Robinson *et al.*, 1998; Moore *et al.*, 1999).

Suspended sediment transport is a continuous process occurring in coastal waters. Many researchers have endeavored to estimate the SPMs in the coastal waters based on the remote sensing reflectance, absorption, and scattered light by water (Tassan and Strum, 1986; Tassan, 1994; Green and Sosik, 2004; Pradhan *et al.*, 2005; Wang *et al.*, 2010; Chauhan *et al.*, 2011; Avinash *et al.*, 2012). Earlier studies about the relationship between SPC and reflectance values in coastal waters suggest that algorithms derived from single band reflectance values may be adopted, where the SPMs increase with increasing reflectance (Curran *et al.*, 1987; Novo *et al.*, 1989).

Later, studies associating the reflectance and water leaving radiance values for different bands were carried out. The single band algorithms have been understood to be the easiest and best possible way e.g., Landsat OLI-TIRS band 4, Landsat TM band 3 or MODIS band 1 (Nellis *et al.*, 1998, Islam *et al.*, 2001, Miller and McKee, 2004, Shi and Wang, 2009). Reflectance in the green and NIR regions has also been proposed e.g. Landsat ETM+ Band 2 (Ouillon *et al.*, 2004) and Band 4 (Ritchie *et al.*, 1990)], but it appears that they are less used. The red band of the visible portion of the spectrum is very sensitive to SPC variations (Schiebe *et al.*, 1992) and is usually used. But the portions of the near-infrared spectrum are also sensitive to SPM thus a combination of several visible and near-infrared bands often produce the strongest SPC-reflectance relationships (Stumpf and Pennock, 1989; Kaliraj *et al.* (2014)). Marine reflectance in a red channel alone can be reliably used to retrieve SPM concentrations (Nechad *et al.*, 2011; Vanhellefont *et al.*, 2013). However, near infrared reflectance in combination with red reflectance (Xia, 1993; Ruhl *et al.*, 2001; Wang *et al.*, 2009) is being used commonly.

Calculating and mapping of Suspended Particulate Matter concentration (SPM), has been routinely done using data from committed wide-swath ocean color instruments such as Orbview-2/SeaWiFS,

Aqua/MODIS and ENVISAT/MERIS (Gohin, 2011; Nechad et al., 2010; Ouillon et al., 2008) as well as freely accessible Landsat ETM and OLI-TIRS (Qu, 2014; Kaliraj, 2014, Cai, et al., 2015).

In general, the optical properties of water–sediment mixtures are highly variable, and many factors such as suspended particle size, shape, and color can affect the water–sediment optics (Baker and Lavelle, 1984; Curran and Novo, 1988; Stumpf and Pennock, 1989; Sydor and Arnone, 1997, Rai and Arunkumar, 2015). Due to these optical complexities, it is difficult to propose a universal algorithm for estimating SPMs. Further, various other parameters such as coastal geomorphology, river input, and local coastal circulation influence the SPMs. Against this background, we endeavored to develop a flexible algorithm for estimation of SPMs using Landsat 8 OLI-TIRS and Landsat 7 ETM+ satellite data by improvising algorithms wherever necessary and required. Specific objectives are as follows:

- Preparation of Algorithm using SCILAB package
- Development of ERDAS Models for processing of remotely sensed images
- Compilation and preparation of SSC maps using ArcMAP software
- Demonstration of the usage of above software package for estimating Suspended Sediment Concentration off Bengal delta.

### **1.1 Theoretical Background**

Atmospheric correction refers to the process of eliminating the contributions by surface glint and atmospheric scattering from the estimated total reflectance to determine the water-leaving reflectance. The total atmospheric reflectance is the sum of the molecular reflectance, called Rayleigh's reflectance, aerosol reflectance, the coupling term, which takes into account the interaction between molecules and aerosols, specular reflection of the sun (ignored as the sun zenith angle is much larger than the viewing zenith angle), reflectance of foam and whitecaps and can be estimated from wind speed using an empirical relationship (again this reflectance ignored as it is largely corrected during the aerosol correction) (Gordon & Wang, 1994). Marine reflectance also known as water-leaving reflectance, defined as the ratio upwelling radiance just above the water-surface divided by the solar downwelling irradiance.

In NIR band, water is highly absorbing, thus, water-leaving radiance is negligible and can be eliminated, allowing direct estimation of aerosol radiance. The near-infrared and red spectral bands prove to be better for mapping medium to relatively high SPM concentrations as per the previous studies. The description of variables, used in following equations, is provided in Table 1.

(1)

$$\rho_{TOA} = \rho_r + \rho_a + \rho_{ra} + \rho_g + t_v t_0 (\rho_w + \rho_{wc})$$

For this study, Equation 1 can be simplified and written as

Algorithm 1: TOA planetary Reflectance or Conversion of DN to Reflectance

$$\rho_{TOA} = \rho_r + \rho_a + t_0 t_v \rho_w \quad (2)$$

Equation 2 is derived from equation 1 by omitting  $\rho_{ra}$ ,  $\rho_g$  and  $\rho_{wc}$  terms. The values provided in the metadata file (.MTL) are used.

$$\rho_\lambda = M_\rho Q_{cal} + A_\rho \quad (3)$$

The correction for Landsat 8 for the solar angle is made for the TOA planetary Reflectance

$$\rho_{TOA} = \frac{\rho_\lambda}{\cos \theta_0} = \frac{\rho_\lambda}{\sin \theta_{SE}}$$

Calculating TOA for Landsat ETM+ (7) using Band 3 (630-690 nm) and Band 4 (770- (4) n) is a two-step method. The DN values are converted to Radiance values using the  $L_{min}$  and  $L_{max}$  spectral radiance scaling factors from the metadata file (.MTL) and then these radiance values are converted to reflectance values.

DN to Radiance:

$$L_\lambda = \frac{(L_{max} - L_{min})}{(Q_{cal}^{MAX} - Q_{cal}^{MIN})} * (Q_{cal} - Q_{cal}^{MIN}) + L_{min} \quad (5)$$

Radiance to Reflectance values:

Equation (5) gives combined surface and atmospheric reflectance of the Earth. In this along with conversion, normalization for solar irradiance is performed.

$$\rho_{TOA} = \frac{\pi \cdot L_\lambda \cdot d^2}{F_0 \cdot \cos \theta_0} \quad (6)$$

Algorithm 2A: Calculating Molecular Reflectance or Rayleigh Reflectance

The Rayleigh reflectance can be defined as scattering of light off the molecules of the air. Equation for estimation of  $\rho_r$ , (Gordon, Brown, & Evans, 1988) is

$$\rho_r = \tau_r \cdot p_r(\theta_0, \theta_v, \Delta\varphi) \cdot (4 \cdot \cos \theta_0 \cdot \cos \theta_v)^{-1} \quad (7)$$

For calculating the Rayleigh reflectance, the Rayleigh transmission function is calculated using equation 8-9.

$$t_o = \exp \left[ - \left( \frac{\tau_r}{2} + \tau_{oz} \right) / \cos \theta_0 \right] \quad (8)$$

$$t_v = \exp \left[ - \left( \frac{\tau_r}{2} + \tau_{oz} \right) / \cos \theta_v \right] \quad (9)$$

Band averaged Rayleigh optical thicknesses (Bodhaine et al. 1999) and Ozone optical thicknesses (Chang et al. 2014) for a standard atmosphere for Landsat 7 and 8 are tabulated (Table 2).

The Rayleigh phase functions of downward and upward radiance need to be computed, for which the scattering angle for the upward and downward directions are calculated from sun-sensor geometry using the equation 10

$$\cos \theta_{\pm} = \pm \cos \theta_0 \cdot \cos \theta_v - \sin \theta_0 \cdot \sin \theta_v \cdot \cos |\varphi_0 - \varphi_v| \quad (10)$$

$P_r(\vartheta)$ , Rayleigh scattering phase function for scattering angle  $\vartheta$ .  $P_r(\theta_+)$  for upward radiance and  $P_r(\theta_-)$  for downward radiance can be calculated using equation 11

$$P_r(\vartheta) = 0.75 \cdot (1 + \cos^2 \vartheta) \quad (11)$$

Where  $\vartheta$  is  $\theta_+$  and  $\theta_-$

The reflectance of light produced when it travels from one medium to another with different refractive indices is known as Fresnel Reflectance, which is calculated for air incident rays on the water with incident angle  $\theta$ .  $r(\theta)$  is calculated for both local zenith angle and viewing zenith angle i.e.  $r(\theta_0)$  and  $r(\theta_v)$ . Since  $\theta_v = 0$  (Nadir for this study)  $r(\theta_v)$  also equals to zero.

$$r(\theta) = 0.5 \left\{ \frac{\sin^2(\theta - \theta_t)}{\sin^2(\theta + \theta_t)} + \frac{\tan^2(\theta - \theta_t)}{\tan^2(\theta + \theta_t)} \right\} \quad (12)$$

$$\theta_t = \sin^{-1}(n_w \sin \theta) \quad (13)$$

Using the above-calculated values, the Rayleigh reflectance value -  $p_r(\theta_0, \theta_v, \Delta\varphi)$  is derived from the equation 14 which is then used in the equation 7 to calculate Rayleigh reflectance value.

$$p_r(\theta_0, \theta_v, \Delta\varphi) = P_r(\theta_-) + [r(\theta_v) + r(\theta_0)] \cdot P_r(\theta_+) \quad (14)$$

Rayleigh correction can be performed by subtracting the Rayleigh reflectance value from the top of atmosphere reflectance.

$$\rho_c = \rho_{TOA} - \rho_r \quad (15)$$

Algorithm 2B: Aerosol Correction and Marine Reflectance Calculation

Aerosol-type ( $\epsilon$ ) is determined from the ratio of reflectance in the band pair, over water pixels where the marine contribution in those bands can be assumed to be zero.  $\epsilon$  The ratio of multiple-scattering aerosol reflectance is constant over the scene. So  $\epsilon$  is taken equal to 1 for more standard processing in VR and NIR band (Vanhellemont et al., 2014).

In VR-NIR (4, 5) the aerosol reflectance is estimated by assuming a linear relationship between marine reflectance of bands 4-5 and constant aerosol type ( $\epsilon$ ) over the scene.  $\epsilon$  can be derived from the slope of the regression line (Neukermans et al., 2009) or the median ratio of Rayleigh corrected reflectance in bands 4 and 5 ( $\rho_c^4, \rho_c^5$ ) over clear water pixels (Vanhellemont et al., 2014).

$\alpha$ , the ratio of marine reflectance in the two bands is constant, here estimated using the average similarity spectrum for the band central wavelengths.

For LANDSAT 8,  $\alpha$  is:

$$\alpha = \frac{\rho_w^{(4)}}{\rho_w^{(5)}} = \frac{\bar{\rho}_{wn780}^{(655nm)}}{\bar{\rho}_{wn780}^{(865nm)}} = \frac{4.734}{0.544} = 8.702 \quad (16)$$

For LANDSAT 7,  $\alpha$  is calculated using equation 16 by replacing values of bands 4, 5 with values of bands 3, 4 which are 4.432 and 0.742 respectively.

$\gamma$  is the ratio of diffused atmospheric transmittances in the two bands. For LANDSAT 8,  $\gamma$  is calculated using band 4 and band 5 by equation 17.

$$\gamma = \frac{t_0^{(4)} t_v^{(4)}}{t_0^{(5)} t_v^{(5)}} \quad (17)$$

Similarly, for LANDSAT 7,  $\gamma$  is calculated using band 3 and band 4 for equation 17.

Marine reflectance using single band algorithm i.e. marine reflectance in band 3 for Landsat 7 and band 4 for Landsat 8 is calculated using  $\rho_w^{(3)}$  and  $\rho_w^{(4)}$  from equation 18.

$$\rho_w^{(3)} = \frac{\alpha}{t_0^{(4)} t_v^{(4)}} \left[ \frac{\rho_c^{(3)} - \rho_c^{(4)}}{\alpha\gamma - \varepsilon} \right] \quad (18)$$

Algorithm 3: Suspended Particulate Matter Concentration calculation

Suspended particulate matter concentration (SPM) is computed from  $\rho_w$  using the single band algorithm (Nechad et al., 2010).

$$SPM = \frac{A\rho_w}{1 - \rho_w/C} \quad (19)$$

In equation 19, for Landsat 8 OLI band 4 (655 nm), the value of A and C are 289.29 g m<sup>-3</sup> & 0.1686 respectively and for Landsat 7 ETM+ band 3 (660 nm) tabulated values are A = 327.84 g m<sup>-3</sup> & C = 0.1708.

Based on the above 19 equations and using SCILAB software, the algorithm is developed for calibrating marine reflectance and measuring Suspended particulate matter concentration (SPM) as per steps indicated in the flowchart (Fig. 1).

## 2. MATERIAL AND METHODOLOGY

Ortho-rectified and terrain corrected Level 1T OLI Landsat 8 and 7 imageries are obtained from USGS Earth Explorer site (<http://earthexplorer.usgs.gov/>). Imageries processed by the Level 1 Product Generation System (LPGS) versions 2.2.2 (up to 2010) and 2.2.3 (beyond 2010) are provided in GeoTIFF format with UTM projection and WGS84 datum. Top of atmosphere reflectance in bands of OLI (4 and 5) and ETM+ (3 and 4) (Table 3), respectively red and near infrared bands are derived. Images are corrected for scattering by molecules (Rayleigh) and aerosols to retrieve water-leaving reflectance,  $\rho_w$  in the red band. Aerosol reflectance is estimated assuming a constant aerosol type over the scene and a constant ratio of water-leaving reflectance for OLI in bands 4 and 5 and for ETM+ in bands 3 and 4 (Table 3) (Vanhellmont et al., 2014). Suspended particulate matter concentrations (SPM) are computed from  $\rho_w$  using equations explained in an earlier section. Adopting equations, an algorithm is written and executed in the SCILAB package. Schematic flowchart of the methodology followed is shown in Figure 1.

### 2.1 SCILAB Package

SCILAB-5.4.1, freely available numerical computation software, was installed and utilized to develop an algorithm for digital estimation of suspended particulate matter concentration. The applicability of this package has been increased further by functions which can calculate various

reflectance values i.e. Top of Atmosphere planetary reflectance, Rayleigh reflectance, Fresnel reflectance, Aerosol reflectance and Water leaving reflectance. These functions have been compiled within one package. The equations described in earlier section have been utilized while developing SCILAB algorithms in this package. Few equations have also been simplified to achieve a precise output. The package can further be converted to a graphic user interface. The algorithm has been made user-friendly using the programming loops for the user defined data set. The algorithm operates on Landsat ETM+ and Landsat OLI-TIRS sensor data. In this study, basic focus is on the band 3, 4 for Landsat ETM+ and band 4, 5 for Landsat OLI-TIRS.

The software developed using SCILAB Package with .sce format is executed to obtain the values of various reflectance and the suitable corrections. The package is formed by a compilation of two functions and conditional loops. On execution of the package, the input values (from the Metadata file (.MTL)) are asked from the user as per the sensor choice. The software calls and runs the suitable function as per the requirement and provides required values.

## **2.2 ERDAS Models for Processing Images**

ERDAS Imagine 2014 by Leica Geo-systems was used for image processing in this study. The Landsat 7 and 8 images were processed for effective estimation of the suspended particulate matter concentration in mg/l. For iterative processing purpose, the models were prepared using the model maker tool. The models gave the quantitative estimation of SPMC, pixel-wise, in the image.

ERDAS Models for processing LANDSAT 8 data:

### Model 1: DN to TOA reflectance

This model converts the DN value to TOA reflectance using Eq. (3) & (4). The two steps of DN conversion to TOA with and without correction for sun angle have been modeled in this. TOA planetary reflectance is obtained for Band 4 & Band 5 in this (L-8) case (Fig. 2).

### Model 2: Obtaining Atmospheric Corrected marine Reflectance

The respective bands obtained from the model 1 (TOA band\_4 and TOA band\_5) are then stacked together using the Layer stacking tool in ERDAS Imagine 2014. The marine reflectance is obtained using this model. This model also incorporates the values of Rayleigh Reflection calculated from the SCILAB package. The function of this model is based on equation (18) (Fig. 3).

### Model 3: SPM Calculation



This model is used to calculate the concentration of suspended sediments for each pixel of the image. The layer obtained from model 2 is used as an input to this model. The function of this model is based on equation (19) with a value of  $A = 289.29 \text{ g m}^{-3}$  and  $C = 0.1686$  (Fig. 4).

ERDAS Models for processing LANDSAT 7 data

Model 4: DN to Radiance values

This model uses the equation (5) for conversion of the DN to Radiance values for Band 3 (630-690 nm) and Band 4 (770-900 nm) (Fig. 5).

Model 5: Radiance to Reflectance values

The image obtained after executing model 4 is used as an input for model 5. The radiance values calculated for the respective bands are converted to reflectance values in this. This model is based on equation (6) (Fig 6).

To estimate marine reflectance and suspended sediment concentration from band 3 & 4 of LANDSAT 7, the same models 2 & 3 used for LANDSAT 8 were applied. For estimating marine reflectance, the respective bands obtained from the model 5 (TOA band\_3 and TOA band\_4) were then stacked together using the Layer Stacking Tool in ERDAS Imagine 2014. The marine reflectance is obtained by using model 2. This model also incorporates the values of Rayleigh Reflection calculated from the SCILAB package. The function of this model is based on equation (18) (Fig. 3). Suspended sediment concentration from band 3 & 4 of LANDSAT 7 is estimated by taking the corrected layer obtained from model 2 as input to model 3. The function of this model is based on equation (19) with the value of  $A = 327.84 \text{ g m}^{-3}$  &  $C = 0.1708$  (Fig. 4)

### **3. ArcMap**

The developed software package is applied for the retrieval of SSC's from Landsat 7 ETM and Landsat 8 data. The outputs of the ERDAS model 3 in the form of processed satellite image are subjected to the ArcMap software of ArcINFO for producing seasonal SSC maps off Bay of Bengal delta region. The Bengal Delta, also known as the Ganges–Brahmaputra Delta (G-B Delta), is a river delta in the South Asia region, including Bangladesh and the state of West Bengal, India. The delta stretches from the Hooghly River on the west to the River Meghna on the east. A number of large rivers flow through the Brahmaputra Delta, including the Padma (a main distributary of the Ganges) and the Jamuna (a main distributary of the Brahmaputra), which merge and then join the Meghna before entering the sea. The delta stretches approximately up to 354 km, is the largest delta in the world that empties into the Bay of Bengal (Fig. 7). This study focuses on the deltaic and off deltaic

region of Bengal delta which stretches from Latitude 22.72194 N and Longitude 87.41873 E to Latitude 22.70087 N and Longitude 89.62919 E.

### **3. RESULTS**

#### **3.1 Result for SCILAB PACKAGE**

The user inputs the value of parameters, which vary with respect to data scene, from the metadata file (.MTL). For Landsat 8, the user needs to input the Quantized and calibrated standard product pixel values (DN), Sun Elevation Angle in degrees and Sun Azimuth Angle in degrees to obtain results. Whereas for Landsat 7, the user has to input the Maximum and Minimum Radiance values (for band 3 and band 4), Quantized and calibrated standard product pixel values (DN), Sun Elevation Angle in degrees, Earth-Sun distance in astronomical unit, Sun Azimuth Angle in degrees and Band averaged solar irradiance. These parameters are necessary elements for further calculations. The algorithm calibrates marine reflectance and measures suspended particulate matter concentration (Fig. 1). Calibrated products of the algorithm are used in developing ERDAS models for processing satellite images.

#### **3.2. Satellite image processing results**

Using the ArcMAP software of ArcInfo, seasonal SPM maps were generated from Landsat 8 OLI-TIRS and Landsat 7 ETM+ satellite data. The Suspended Particulate Matter Concentration (mg/l) is estimated from Landsat 8 OLI-TIRS and Landsat 7 ETM+ satellite data using one cloudless image per month, for the year 2014 and year 2010 respectively. The output SPM images are then expressed in the form of a map using ArcMAP with total 23 classes at an interval of 3 (Fig. 10, 11, 12). The values of the SPM are then observed from the different colors of the color ramp to find the maximum concentration range for the scene. The location of higher values of SPM can also be witnessed from the map. Table 1 shows the maximum range of SPM in the scene with respect to a particular date and time. Generated maps for Landsat 8 images are assembled in Fig. 10, 11, 12.

From Landsat 7 data, maps are generated in a similar manner (Fig. 8 & 9). Landsat 7 data utilized is 4 years older than Landsat 8 data. The images for all the months could not be acquired either due to unavailability of data or due to cloud cover. Table 2 shows the maximum range of SSC in the scene with respect to particular date and time.

### **4. DISCUSSION**

The entire package includes a combined work of SCILAB, ERDAS, and ArcMAP. The package has been made flexible by forming different modules for different corrections to be used for other

sensors. The sensor-specific constants can be simply changed in the respective module of the package leaving the rest of the package functional. The package has been developed for fixed aerosol type over the scene because the aerosol correction is a big task in itself due to its rapid variation with space and time.

Availability of repetitive, synoptic and multi-spectral data from various satellite platforms is helpful in generating information on varied aspects of the coastal and near-shore environment, including sources, sinks, transport path, sediment dynamics etc. In the present study, highest sediment concentration is observed during May (60-63 mg/l) (Fig. 9) and lowest during December (21-24 mg/l) (Fig. 9) when measured by ETM (Landsat 7) data while highest concentration was during July (above 69 mg/l) (Fig. 11) and lowest during January 2015 (30-33 mg/l) (Fig. 12) when measured by OLI-TIRS data (Landsat 8). In the case of both data sets, sediment plumes are mostly pointed southwards and later SE or SW wards generating sand shoals perpendicular to coasts. During some months (like August) (Fig. 11) concentration is very low due to the presence of cloud cover.

The results of the study using Landsat 8 shows the higher value of suspended sediment concentration for the month of July, owing to the fact that July is a monsoon month, the river flow and discharge increases leading to a much higher rate of sediment transport along the rivers. The image for August month could not be processed to the best of its reflectance due to clouds. Cloud removal techniques like F-mask can be applied for cloud and its shadow masking. Just after the monsoon, the suspended sediment concentration is observed to be much higher.

The results of the study using Landsat 7 show much higher suspended sediment in May. The processing of Landsat 7 images can be done more effectively by the gap filling techniques prior to any processing. Though gap filling is less reliable, in some scenarios, it can be used for a better output. The month of November also has a good amount of sediments. The study of Landsat 7 could not be done for monsoon and post-monsoon season due to non-availability of cloud-free data.

The software package is developed using windows 7 and can run on windows 8 and above. The algorithm is successfully implemented in Indian west coast water (less turbidity) as well as in east coast water (high turbidity) and off Ganga-Brahmaputra delta coast (very high turbidity). The present software pack requires less than 5 minutes of CPU time to process one image and no special hardware is required. Future work would include the development of algorithm extension to extreme types of waters, mobile applications for various purpose and inclusion of “user defined models”.

The present study helps in understanding the quantum and dispersal direction of the suspended sediments in the coastal waters of India, which in turn will help in coastal zone supervision and

upkeep of navigational channels. This software package can be used to derive information about water components (optical properties, particulate concentrations) from the estimated radiance off the water surface. Such facts are beneficial for the management of water quality, monitoring of water pollution, modeling of sediment dispersal and movement and sediment budgeting in coastal environments.

## **5. CONCLUSIONS**

Based on the ongoing discussion, it may be concluded that

1. The study of suspended sediment concentration and transport has been made much easier using the satellite imagery due to continuous and synoptic view. Temporal satellites monitoring of the area offers a better opportunity for the monthly, seasonal and yearly study of the suspended sediments.
2. Freely downloadable SCILAB software package is suitable for computing different atmospheric corrections and other parameters from Landsat ETM+ and Landsat OLI-TIRS.
3. The software flexibility accommodates other remotely sensed data like Ocean Color monitor (OCM) data, MODIS data etc. and estimates suspended sediment concentration in coastal waters, by replacing a few parameters in the algorithm.
4. It is advisable to use Landsat 8 OLI-TIRS data rather than Landsat ETM and ETM+ data for the study region, due to data gaps in Landsat ETM+ and secondly due to limited availability of good quality data.
5. The present study assisted in knowing the quantum and dispersal patterns of the suspended sediments in the Bay of Bengal region, which in turn; will support coastal zone management and conservation of navigational channels.

## **ACKNOWLEDGEMENTS**

We express our sincere gratitude to Director, CSIR-National Institute of Oceanography for permitting us to publish this material. The first author carried out this study in NIO as summer intern student under 2nd author's guidance. The first author wishes to extend her sincere gratitude to Dr. D.K Gupta (HOD) and Dr. Saurabh Mittal, Asst. Prof, Department of Petroleum Engineering and Earth Sciences, University of Petroleum and Energy Studies, Dehradun, for the permission to pursue this summer internship program and their unforgettable help and assistance. Landsat 8 OLI-TIRS

data, Landsat 7 ETM, and ETM+ data are downloaded from <http://earthexplorer.usgs.gov/>. This is the contribution number ----- of National Institute of Oceanography, Council of Scientific and Industrial Research (CSIR), Goa, India. We wish to express our gratitude to the anonymous reviewers for their insightful comments on this manuscript.

### References:

Avinash, K., Babula J., Vinaya, M.S., Jayappa, K.S., Narayana, A.C. and Gangadhara Bhat, H., 2012. Regionally tuned algorithm to study the seasonal variation of suspended sediment concentration using IRS-P4 Ocean Colour Monitor data. *Egypt J. Remote. Sens. and Space Sci.*, **15**, 67-81.

Baker, E.T., Lavelle, J. W., 1984. The effect of particle size on the light attenuation coefficient of natural suspensions. *J. Geophys. Res.*, **89**, 8197–8203.

Bodhaine, B.A., Wood, N.B., Dutton, E.G., Slusser, J.R., 1999. On Rayleigh optical depth calculations, *Journal of Atmospheric and Oceanic Technology*, **16**, 1854–1861.

Cai, LiNa, DanLing Tang, CongYing Li, 2015. An investigation of spatial variation of suspended sediment concentration induced by a bay bridge based on Landsat TM and OLI data, *Advances in Space Research*, **56**(2), 293-303.

Chang J.H.W., Dayou, J., Sentian, J., 2014. Development of a Near-Sea-Level Calibration Algorithm for Aerosol Optical Depth Measurement Using a Ground-Based Spectrometer. *Aerosol and Air Quality Research*, **14**, 386–395.

Chauhan, O.S., Raghavan, B.R., Khushvir Singh, Rajawat, A.S., Ajai Kader, U.S.A. and Nayak, S., 2011. Influence of orographically enhanced SW monsoon flux on coastal processes along the SE Arabian Sea. *J. Geophys. Res.*, **116**, C12037.

Curran, P.J., Wilkinson, H.D., 1985. Mapping the concentration and dispersal pattern of dye from a long sea outfall using digitized aerial photography, *I. J. Remote Sens.*, **6**, 17-31.

Curran, P.J., Hansom, J.D., Plummer, S.E., Pedley, M.I., 1987. Multispectral remote sensing of near shore suspended sediments: A pilot study. *Int. J. Remote Sens.*, **8** (1), 103-112.

Curran, P.J., Novo, E.M.M., 1988. The relationship between suspended sediment concentration and remotely sensed spectral radiance: a review. *J. Coast. Res.*, **4**(3), 351–368.

Gohin, F., 2011. Annual cycles of chlorophyll-a, non-algal suspended particulate matter, and turbidity observed from space and in-situ in coastal waters, *Ocean Science*, **7**, 705–732.

Gordon, H.R., Brown, J.W., Evans, R.H., 1988. Exact Rayleigh scattering calculations for use with the Nimbus-7 Coastal one Color Scanner. *Applied Optics*, **27**, 862-87.

Gordon, H.R., Wang, J.J., 1994. Influence of oceanic whitecaps on atmospheric correction of SeaWiifs, *Applied optics*, **33**, 7754-7763.

Green, R.E., Sosik, H.M. (2004). Analysis of apparent optical properties and ocean color models using measurements of seawater constituents in New England continental shelf surface waters. *J. Geophys. Res.*, **109** (C3).

- Islam, M.R., Yamaguchi, Y., Ogawa, K., 2001. Suspended sediment in the Ganges and Brahmaputra rivers in Bangladesh: Observation from TM and AVHRR data, *Hydrol. Processes*, 15,493–509.
- Kaliraj, S., Chandrasekar, N., Mangesh N.S, 2014. Multispectral image analysis of suspended sediment concentration along the Southern coast of Kanyakumari, Tamil Nadu, India. *Journal of Coastal Research* 1, 63-67.
- Mckim, H.L., Merry, C.J., Layman, R.W., 1984. Water quality monitoring using an airborne spectroradiometer. *Photogrammetric Engineering and Remote Sens.*, 50, 353-360.
- Miller, R.L., McKee, B.A. 2004. Using MODIS Terra 250 m imagery to map concentrations of total suspended matter in coastal waters. *Remote Sensing of Environment* 93, 259–266.
- Moore, G.F., Aiken, J., Lavender, S.J., 1999. The Atmospheric correction of water colour and the quantitative retrieval of suspended particulate matter in case 2 waters: application to MERIS. I. *J. Remote Sens.*, 20, 1713–1733.
- Nechad, B., Alvera-Azcarate, A., Ruddick, K., Greenwood, N., 2011. Reconstruction of MODIS total suspended matter time series maps by DINEOF and validation with autonomous platform data. *Ocean Dynamics*, 61, 1205–1214.
- Nechad, B., Ruddick, K., Park, Y. 2010. Calibration and validation of a generic multi-sensor algorithm for mapping of total suspended matter in turbid waters. *Remote Sensing of Environment*, 114, 854–866.
- Nellis, M.D., Harrington, J.A., Wu, J., 1998. Remote sensing of temporal and spatial variations in pool size, suspended sediment, turbidity, and Secchi depth in Tuttle Creek Reservoir, Kansas: 1993, *Geomorphology*, 21, 281–293.
- Neukermans, G., Ruddick, K., Bernard, E., Ramon, D., Nechad, B., Deschamps, P.Y., 2009. Mapping total suspended matter from geostationary satellites: a feasibility study with SEVIRI in the Southern North Sea. *Opt. Express* 17, 14029–14052.
- Novo, E.M.M., Hansom, J.D., Curran, P.J., 1989. The Effect of viewing geometry and wavelength on the relationship between reflectance and suspended sediment concentration. *Int. J. Remote Sens.*, 10 (8), 1357-1372.
- Ouillon S, Douillet P, Andre´fouet S., 2004. Coupling satellite data with in situ measurements and numerical modeling to study fine suspended sediment transport: a study for the lagoon of New Caledonia. *Coral Reefs*, 23, 109–122.
- Ouillon, S., Douillet, P., Petrenko, A., Neveux, J., Dupouy, C., Froidefond, J.M., 2008. Optical algorithms at satellite wavelengths for total suspended matter in tropical coastal waters. *Sensors*, 8, 4165–4185.
- Pradhan, Y., Thomaskutty, A.V., Rajawat, A.S., Nayak, S.R., 2005. Improved regional algorithm to retrieve total suspended particulate matter using IRS-P4 ocean Colour Monitor data. *J. Opt. A: Pure Appl. Opt.*, 7, 343–349.
- Qu, Liqin, 2014. Remote Sensing Suspended Sediment Concentration in the Yellow River"(2014). *Doctoral Dissertations*. Paper 383.
- Rai, Anant Kr., Arunkumar, 2015. Continuous measurement of suspended sediment concentration: Technological advancement and future outlook, *Measurement*, 76, 209-227.
- Ritchie, J.C., Cooper, C.M., Schiebe, F.R., 1990. The relationships of MSS and TM digital data with suspended sediments, chlorophyll and temperature in Moon Lake, Mississippi. *Remote Sens. Environ* 33,137–14.

- Robinson, M.C., Morris, K.P., Dyer, K.R., 1998. Deriving fluxes of suspended particulate matter in the Humber estuary, UK, using airborne remote sensing. *Mar. Pollut. Bulle.* 37, 155–163.
- Ruhl, C.A., Schoellhamer, D.H., Stumpf, R.P., Lindsay, C.L., 2001. Combined use of remote sensing and continuous monitoring to analyse the variability of suspended-sediment concentrations in San Francisco Bay, California. *Estuarine, Coastal and Shelf Science* 53, 801–812.
- Schiebe F.R., Harrington Jr., J.A., Ritchie, J.C., 1992. Remote sensing of suspended sediments: The Lake Chicot, Arkansas project, *Int. J. Remote Sens.*, 13(8), 1487–1509.
- Shi, W., Wang M., 2009. Satellite observations of flood-driven Mississippi River plume in the spring of 2008, *Geophys. Res. Lett.*, 36, L07607.
- Stumpf, R.P., Pennock, J.R. 1989. Calibration of a general optical equation for remote sensing of suspended sediments in a moderately turbid estuary, *J. Geophys. Res. Oceans*, 1978–2012 (94), 14363–14371.
- Sydor, M., Arnone, R.A., 1997. Effect of suspended particulate and dissolved organic matter on remote sensing of coastal and riverine waters. *Appl. Optics*, 36, 6905–6912.
- Tassan, S., 1994. Local algorithm using SeaWiFS data for retrieval of phytoplankton pigment, suspended sediments and yellow substance in coastal waters. *Appl. Optics*, 12, 2369-2378.
- Tassan, S. and Strum, B., 1986. An algorithm for the retrieval of sediment in turbid coastal waters from CZCS data. *Int. J. Remote Sens.*, 7, 643–655.
- Van der Woerd, H., Pasterkamp, R., 2004. Mapping of the North Sea turbid coastal waters using SeaWiFS data. *Canadian Journal of Remote Sensing*, 30, 44–53
- Vanhellemont, Q., Greenwood, N., Ruddick, K., 2013. Marine reflectance spectra and several standard L2 products from MERIS satellite for point MERIS\_1, RS\_LIVB\_MERIS\_RR3\_12.3b. *Royal Netherlands Institute for Sea Research*, In: Vanhellemont, Q et al. (2013): A benchmark dataset for the validation of MERIS and MODIS ocean color turbidity and PAR attenuation algorithms using autonomous buoy data. Royal Belgian Institute of Natural Sciences.
- Vanhellemont, Q., Neukermans, G., Ruddick, K., 2014. Synergy between polar-orbiting and geostationary sensors: Remote sensing of the ocean at high spatial and high temporal resolution. *Remote Sens. Environment*, 146, 49–62.
- Wang, J.J., Lu, X.X., Liew, S.C., Zhou, Y., 2009. Retrieval of suspended sediment concentrations in large turbid rivers using Landsat ETM plus: an example from the Yangtze River, China. *Earth Surface Processes and Landforms* 34, 1082-1092.
- Wang, J. J., Lu, X. X., Liew, S. C., Zhou, Y., 2010. Remote sensing of suspended sediment concentrations of large rivers using multi-temporal MODIS images: an example in the Middle and Lower Yangtze River, China. *Int. J. Remote Sens.*, 31, 1103-1111.
- Xia, L., 1993. A united model for quantitative remote sensing of suspended sediment concentration, *Int J Rem Sens.* 14(14), 2665–2676.

Table 1. Glossary of variables and their description

<b>Variables</b>	<b>Description</b>	<b>Units</b>
$\rho_{TOA}$	<i>Top of Atmosphere Planetary Reflectance</i>	Unitless
$\rho_r$	<i>Reflectance due to Rayleigh Scattering by air molecules</i>	Unitless
$\rho_a$	<i>Reflectance due to scattering by Aerosol</i>	Unitless
$\rho_{ra}$	<i>Rayleigh and Aerosol interaction Reflectance</i>	Unitless
$\rho_g$	<i>Specular reflectance (glint) of the sun</i>	Unitless
$t_0$	<i>Sun – Sea diffuse transmittance</i>	Unitless
$t_v$	<i>Sea – Sensor diffuse transmittance</i>	Unitless
$\rho_w$	<i>Marine Reflectance</i>	Unitless
$\rho_{wc}$	<i>Reflectance due to foam and white caps</i>	Unitless
$\rho_\lambda$	<i>TOA planetary Reflectance without solar angle correction</i>	Unitless
$M_\rho$	<i>Band multiplicative rescaling factor</i>	Unitless
$Q_{cal}$	<i>Quantized and calibrated standard product pixel values (DN)</i>	Unitless
$A_\rho$	<i>Band specific additive rescaling factor</i>	Unitless
$\theta_{SE}$	<i>Local Sun Elevation Angle</i>	degrees
$\theta_0$	<i>Local Solar Zenith Angle (90 – Sun Elevation Angle)</i>	degrees
$L_\lambda$	<i>Spectral Radiance at the sensor's aperture</i>	$W/(m^2 * sr * \mu m)$
$Q_{cal}^{MAX}$	<i>Maximum quantized calibrated pixel value</i>	Unitless
$Q_{cal}^{MIN}$	<i>Minimum quantized calibrated pixel value</i>	Unitless
$L_{max}$	<i>Spectral radiance scaled to <math>Q_{cal}^{MAX}</math></i>	$W/(m^2 * sr * \mu m)$
$L_{min}$	<i>Spectral radiance scaled to <math>Q_{cal}^{MIN}</math></i>	$W/(m^2 * sr * \mu m)$
$\rho$	<i>planetary reflectance</i>	Unitless
$d$	<i>Earth – sun distance</i>	au
$F_0$	<i>Mean solar exo-atmospheric irradiances</i>	$W/(m^2 * \mu m)$
$\tau_r$	<i>Band averaged Rayleigh optical thickness for a standard atmosphere</i>	Unitless
$\tau_{oz}$	<i>Band averaged Ozone optical thickness for a standard atmosphere</i>	Unitless
$\theta_v$	<i>Viewing Zenith Angle</i>	degrees
$\varphi_0$	<i>Sun Azimuth angle</i>	degrees
$\varphi_v$	<i>Sensor Azimuth angle</i>	degrees
$P_r(\vartheta)$	<i>Rayleigh scattering phase function for scattering angle <math>\vartheta</math></i>	degrees
$P_r(\theta_+)$	<i>For upward radiance</i>	degrees
$P_r(\theta_-)$	<i>For downward radiance</i>	degrees
$\theta_t$	<i>Angle of transmittance</i>	degrees
$n_w$	<i>Refractive index of water w.r. t air, 1.34</i>	Unitless
$\gamma$	<i>Ratio of diffused atmospheric transmittances in the two bands</i>	Unitless
$\alpha$	<i>Ratio of marine reflectance in the two bands</i>	Unitless



Table 2 :  $\tau_r$  and  $\tau_{oz}$  Values for different bands of ETM+ and OLI-TIRS sensors.

<b>SENSOR</b>	<b>BAND</b>	<b>Spectral range</b>	<b>Central wavelength</b>	$\tau_r$	$\tau_{oz}$
ETM+	Band 3(Red)	630-690 nm	660 nm	0.0462	0.0006044
	Band 4(NIR)	770-900 nm	835 nm	0.0179	0.000273
OLI-TIRS	Band 4 (Red)	640-670 nm	655 nm	0.0479	0.0182
	Band 5 (NIR)	850-880 nm	865 nm	0.0155	0.000643

Table 3. Description of data used in this study and range of SSC in mg/l.

<b>DOA</b>	<b>PRODUCT ID</b>	<b>SATELLITE ID</b>	<b>SENSOR</b>	<b>TIME</b>	<b>Range of SSC(mg/l)</b>
29-Jan-2010	LE71380452010029PFS00	Landsat 7	ETM+	4:23:06	30-33
14-Feb-2010	LE71380452010045SGS00	Landsat 7	ETM+	4:23:18	42-45
18-Mar-2010	LE71380452010077PFS00	Landsat 7	ETM+	4:23:32	30-33
3-Apr-2010	LE71380452010093SGS00	Landsat 7	ETM+	4:23:36	36-39
5-May-2010	LE71380452010125SGS00	Landsat 7	ETM+	4:23:34	60-63
13-Nov-2010	LE71380452010317ASN00	Landsat 7	ETM+	4:24:05	45-48
31-Dec-2010	LE71380452010365PFS00	Landsat 7	ETM+	4:24:33	21-24
1-Feb-2014	LC81380452014032LGN00	Landsat 8	OLI-TIRS	4:32:27	36-39
6-Apr-2014	LC81380452014096LGN00	Landsat 8	OLI-TIRS	4:31:33	48-51
8-May-2014	LC81380452014128LGN00	Landsat 8	OLI-TIRS	4:31:01	39-42
9-Jun-2014	LC81380452014160LGN00	Landsat 8	OLI-TIRS	4:31:04	33-36
11-Jul-2014	LC81380452014192LGN00	Landsat 8	OLI-TIRS	4:31:15	69+
28-Aug-2014	LC81380452014240LGN00	Landsat 8	OLI-TIRS	4:31:28	36-39
29-Sep-2014	LC81380452014272LGN00	Landsat 8	OLI-TIRS	4:31:32	63-66
31-Oct-2014	LC81380452014304LGN00	Landsat 8	OLI-TIRS	4:31:34	45-48
16-Nov-2014	LC81380452014320LGN00	Landsat 8	OLI-TIRS	4:31:36	45-48
18-Dec-2014	LC81380452014352LGN00	Landsat 8	OLI-TIRS	4:31:31	42-45
19-Jan-2015	LC81380452015019LGN00	Landsat 8	OLI-TIRS	4:31:23	30-33

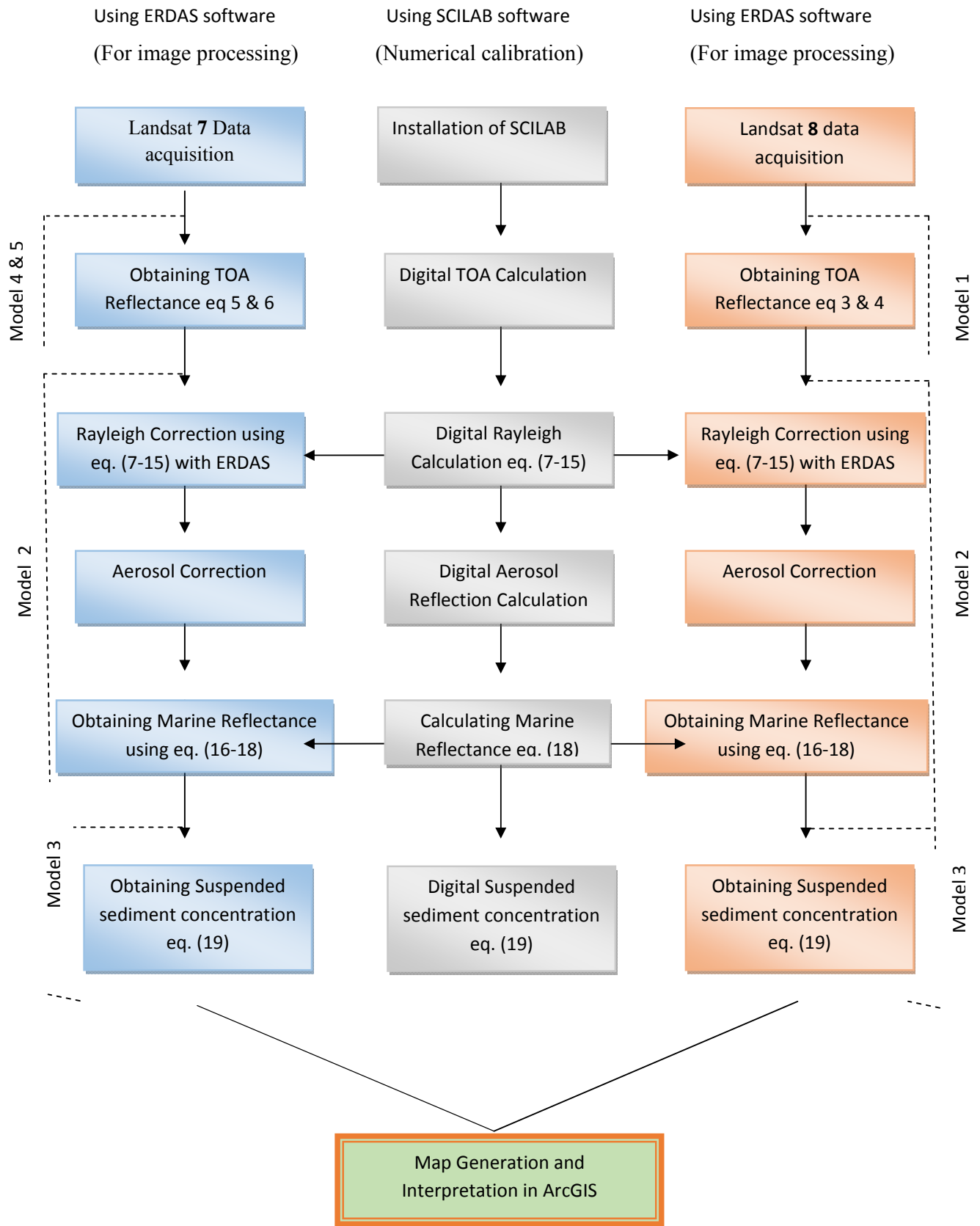


Fig. 1. Schematic Flowchart of Methodology

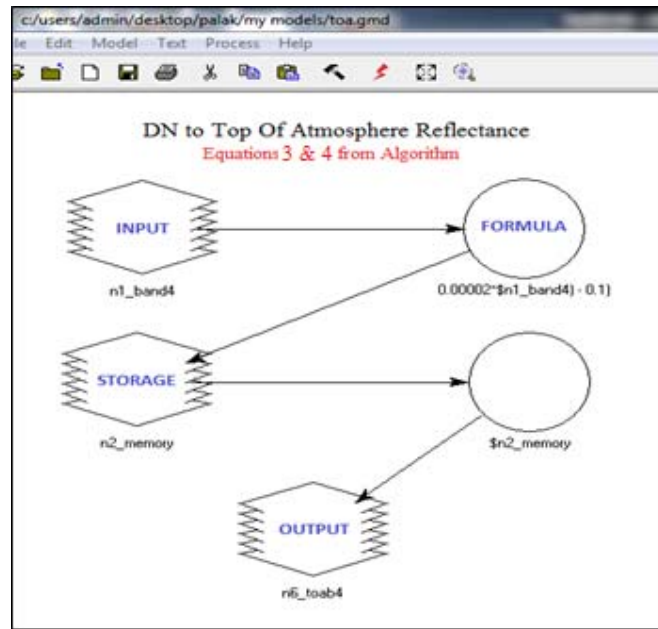


Fig. 2. Model 1 for calibrating Top of atmospheric reflectance from Landsat 8 DN values using equations 3 & 4.

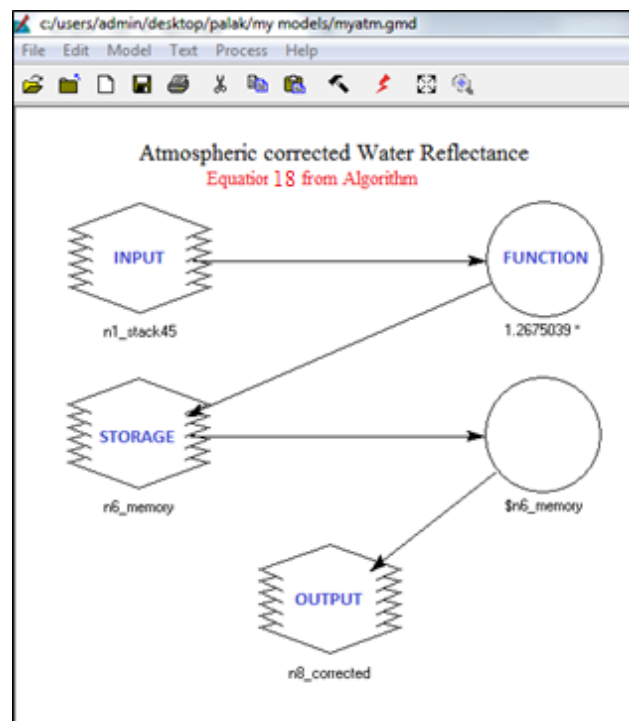


Fig. 3. Model 2 calibrates marine reflectance from Top of atmospheric reflectance stacked bands obtained from model 1 using equations 18.

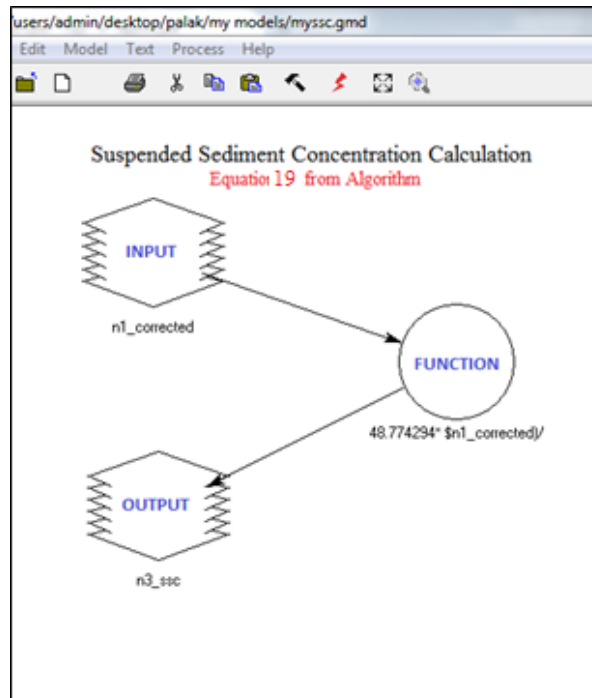


Fig. 4. Model 3 estimates suspended sediment concentration from marine reflectance derived from Landsat 8 DN values using equations 19.

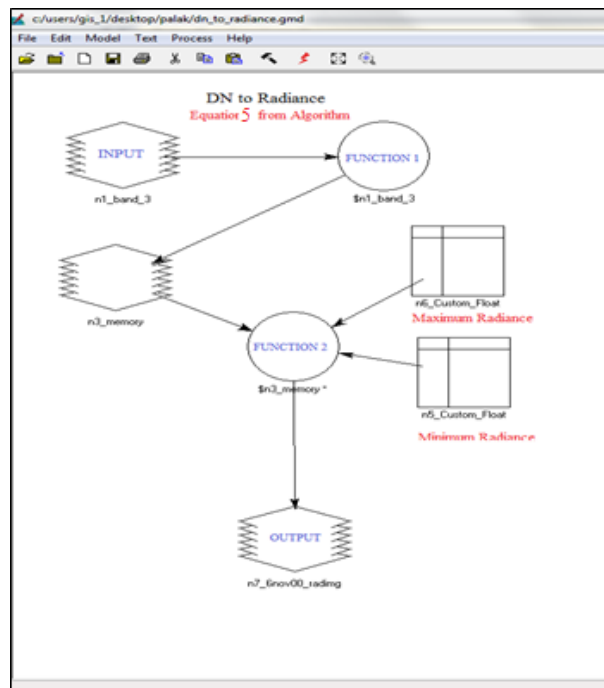


Fig. 5. Model 4 converts DN values of band 3 & 4 of LANDSAT 7 to Radiance values as per equation 5.

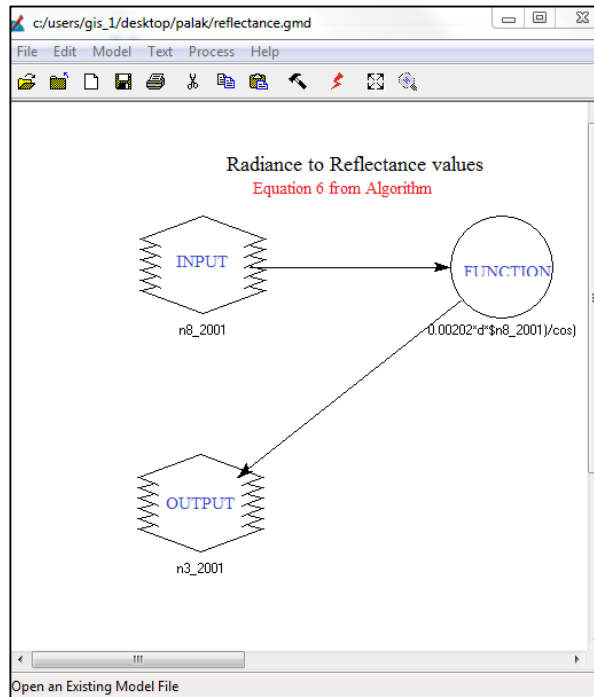


Fig. 6. Model 5 converts Radiance values of band 3 & 4 of LANDSAT 7 derived from model 1 to Reflectance values according to equation 6.

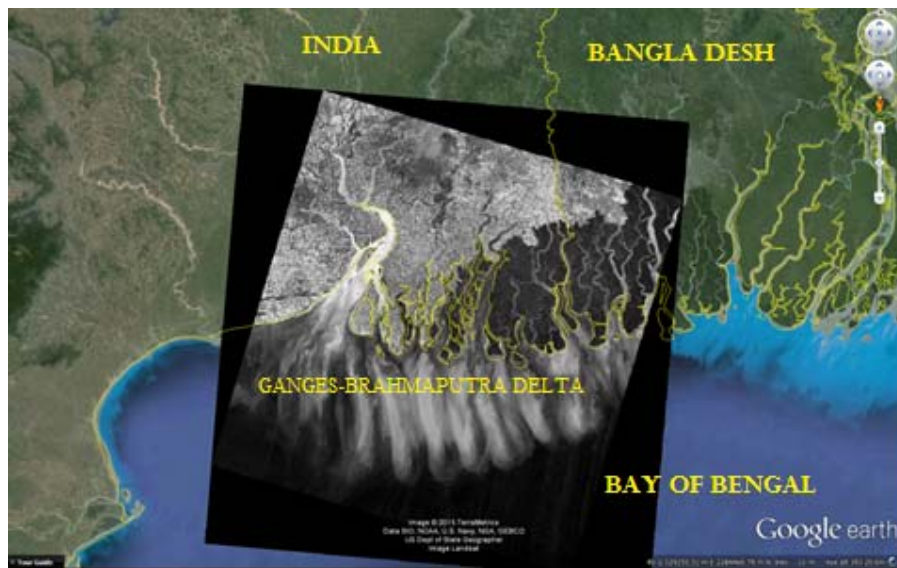


Fig. 7. Satellite image covering study area - Ganges-Brahmaputra Delta, overlapped on Google earth map.

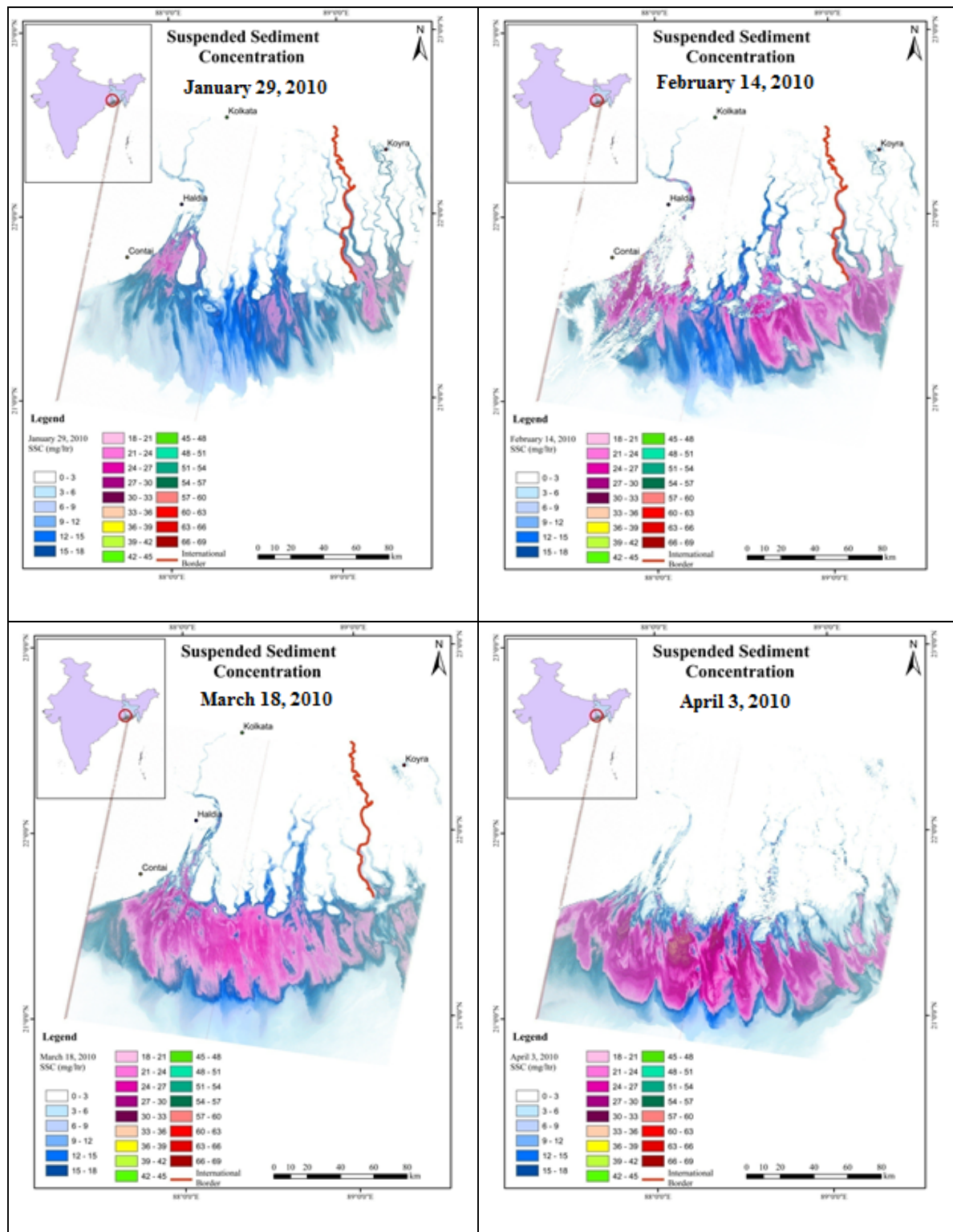


Fig. 8. Suspended sediment concentration for January, February, March & April months of 2010.

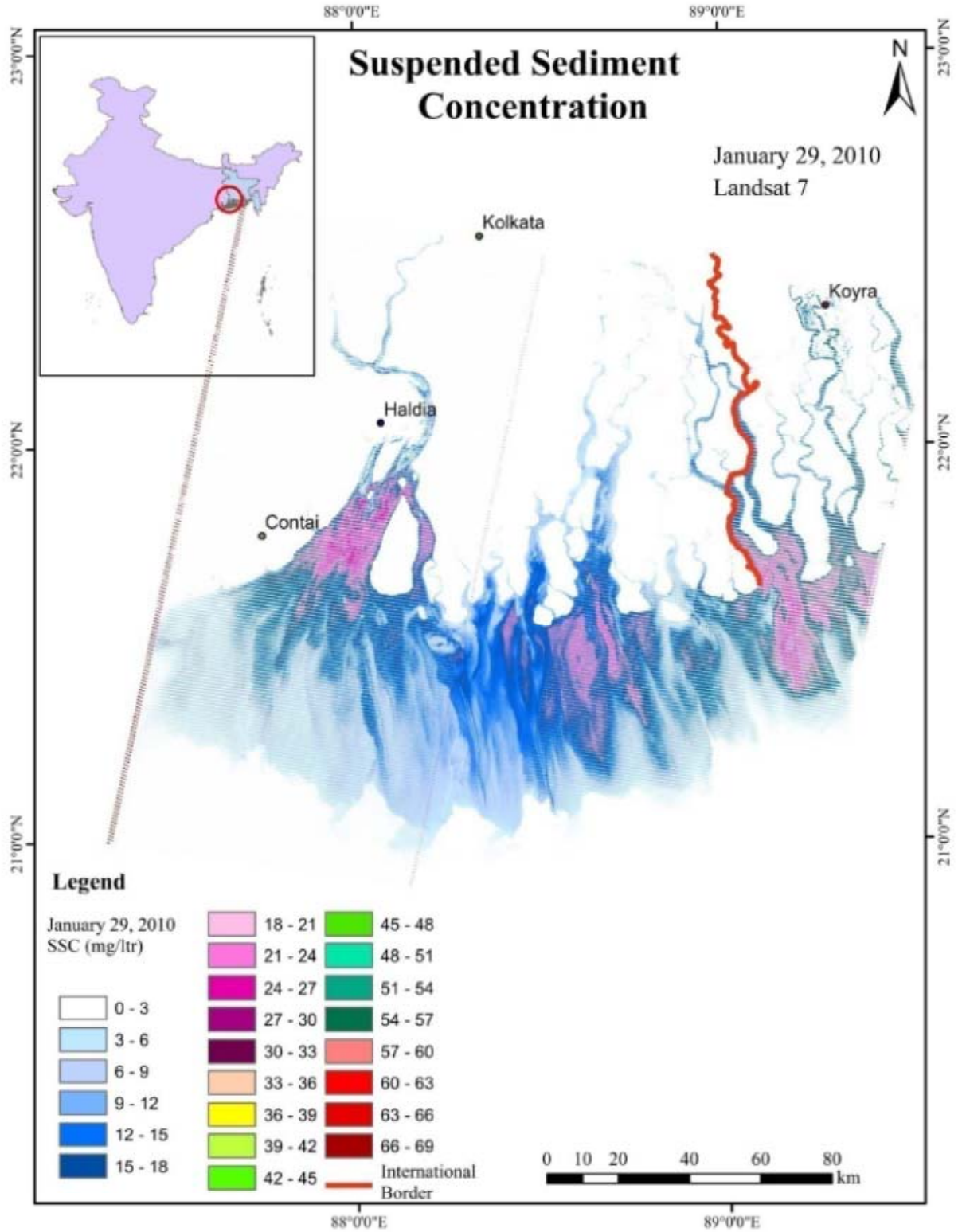


Fig. 8. 1. Suspended sediment concentration (mg/l) in the study area January 29, 2010.



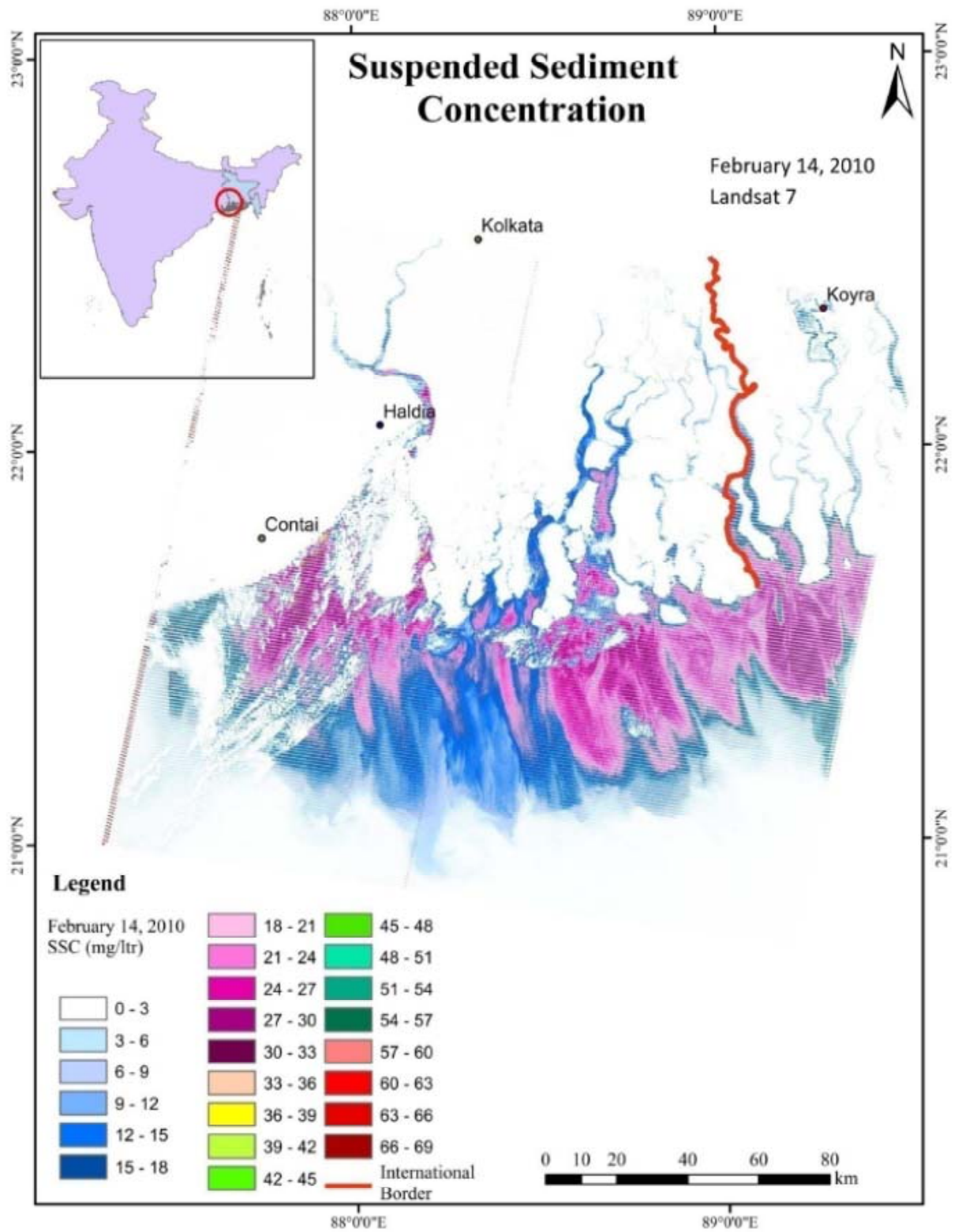


Fig. 8. 2. Suspended sediment concentration (mg/l) in the study area on February 14, 2010.



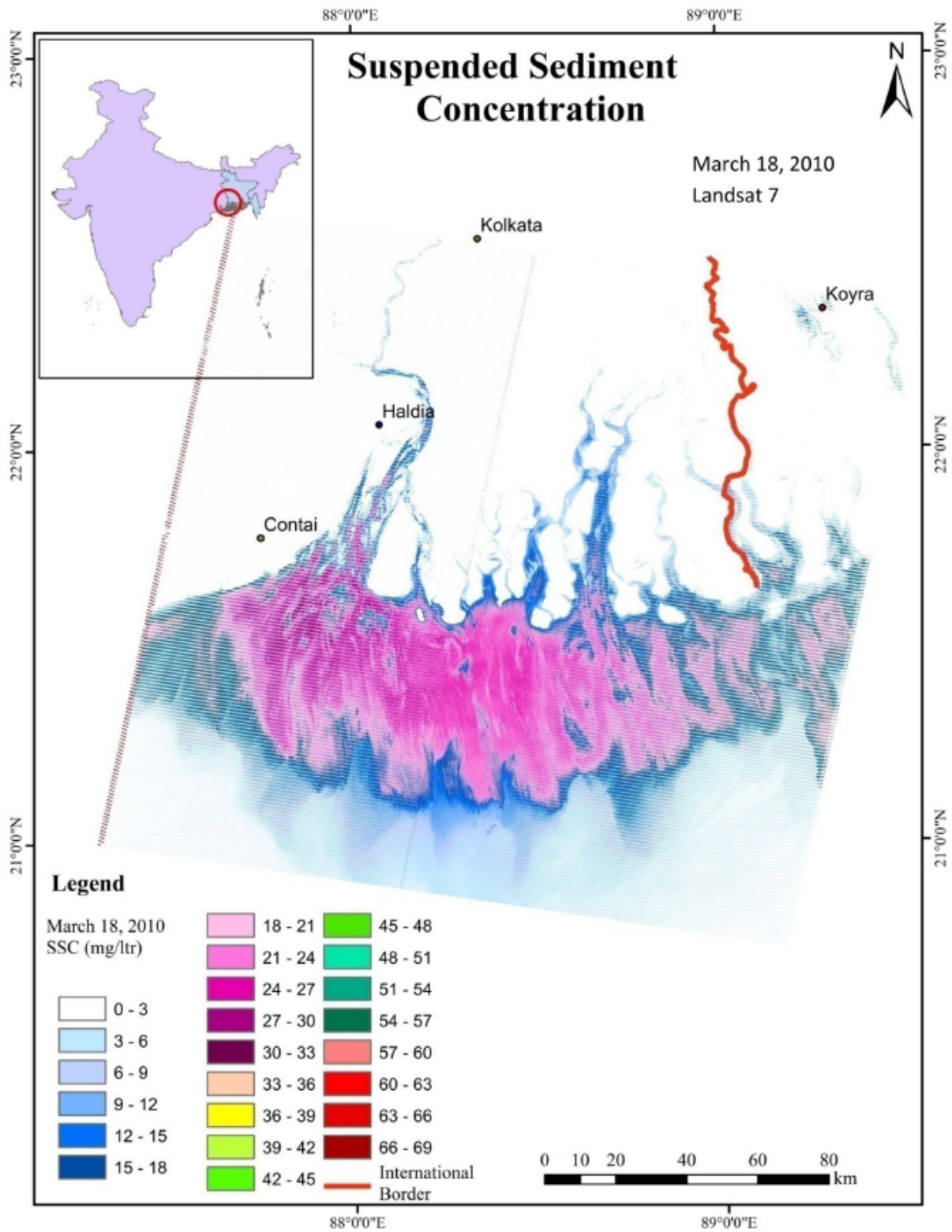


Fig. 8. 3. Suspended sediment concentration (mg/l) in the study area on March 18, 2010.

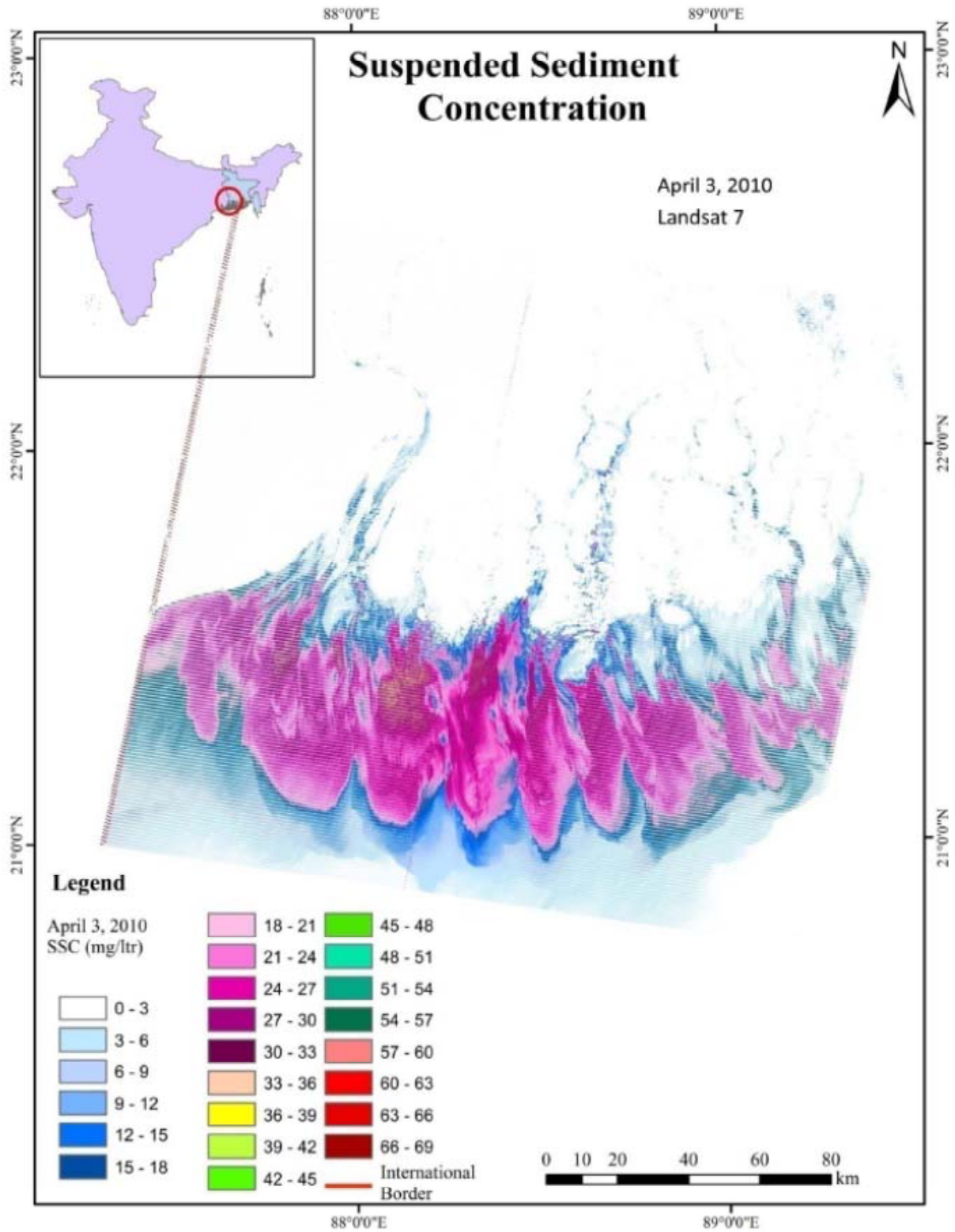


Fig. 8. 4. Suspended sediment concentration (mg/l) in the study area on April 3, 2010.

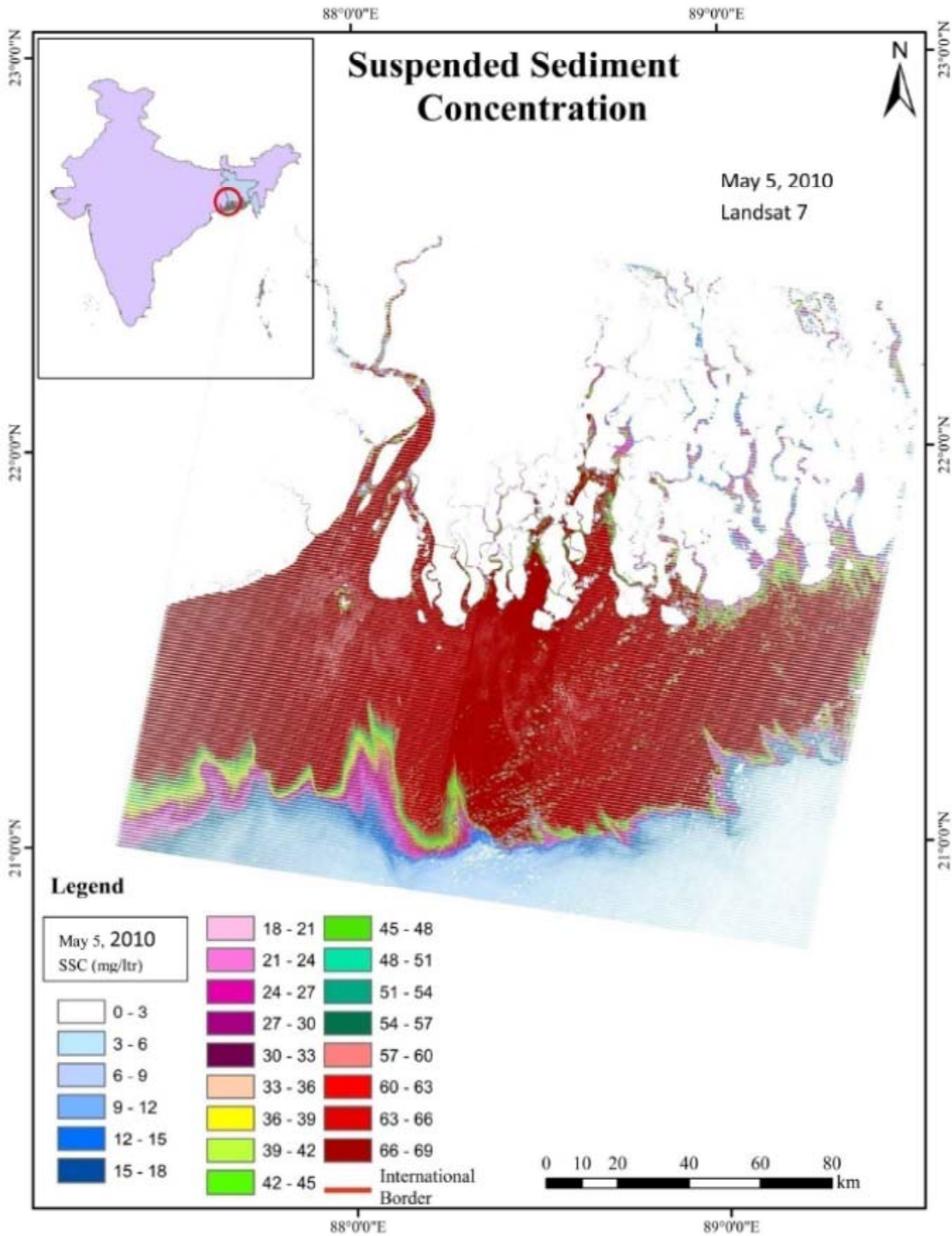


Fig. 9. 1. Suspended sediment concentration (mg/l) in the study area on May 5, 2010.

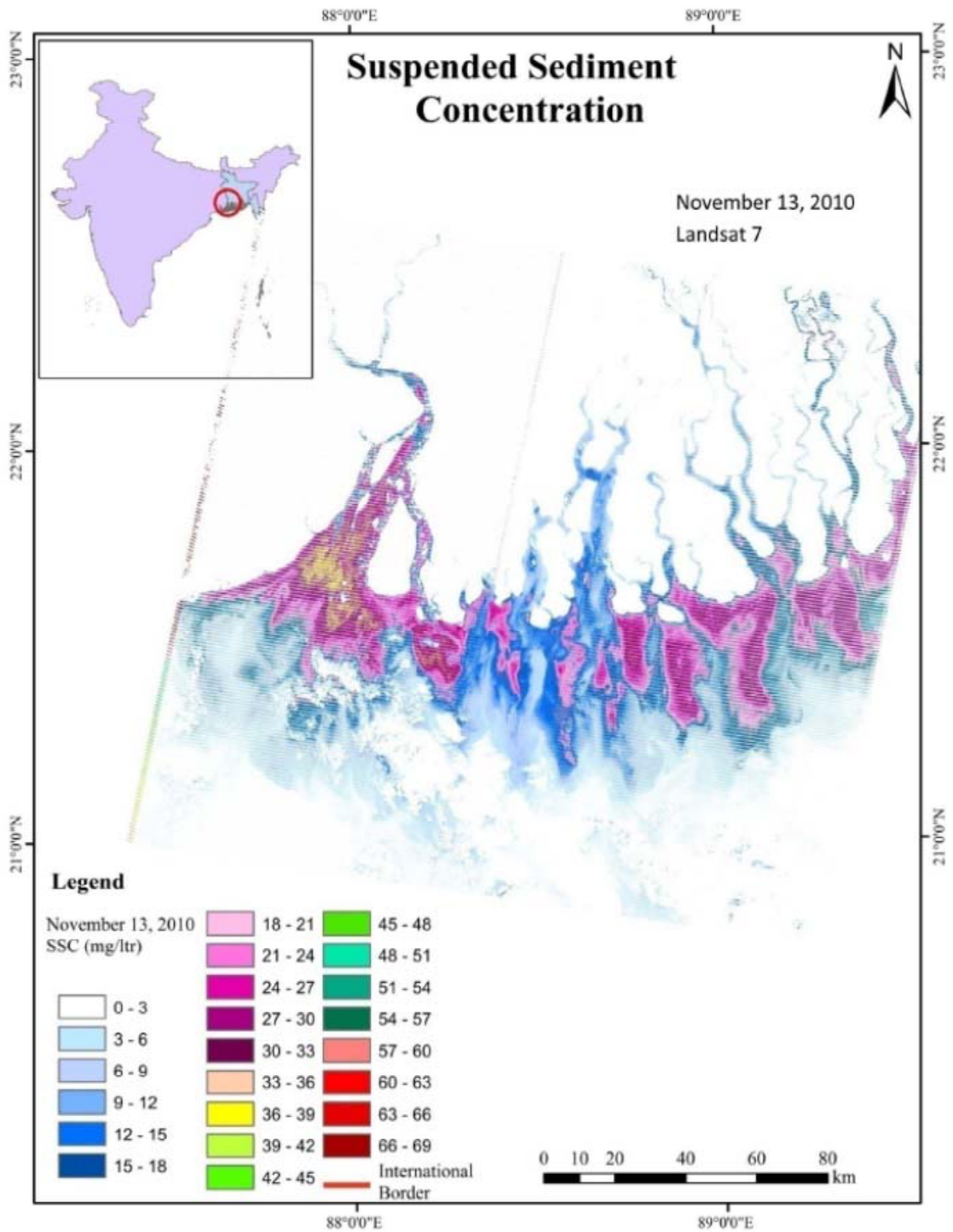


Fig. 9. 2. Suspended sediment concentration (mg/l) in the study area on November 13, 2010.



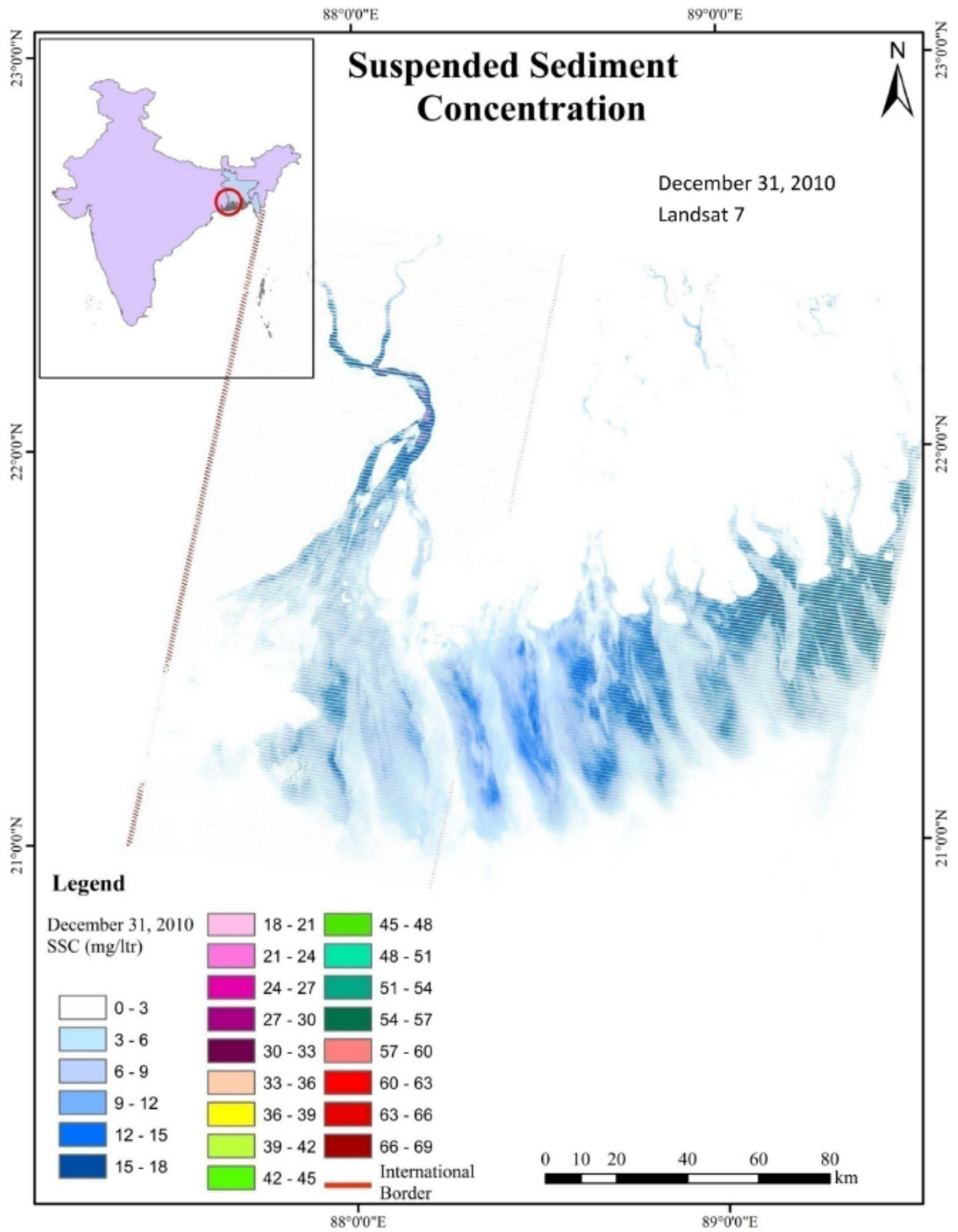


Fig. 9. 3. Suspended sediment concentration (mg/l) in the study area on December 31, 2010.

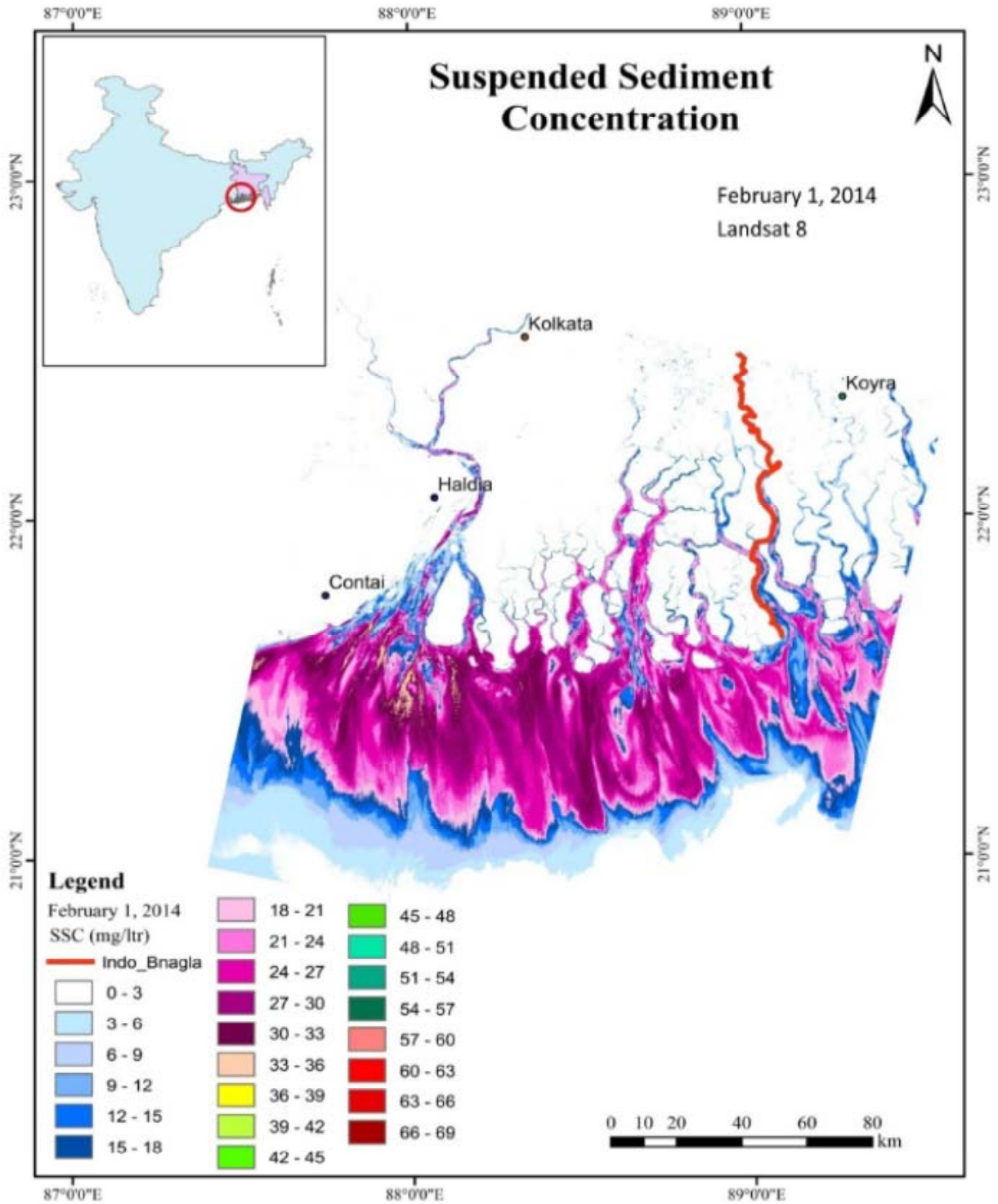


Fig. 10.1. Suspended sediment concentration (mg/l) in the study area on February 1, 2010.

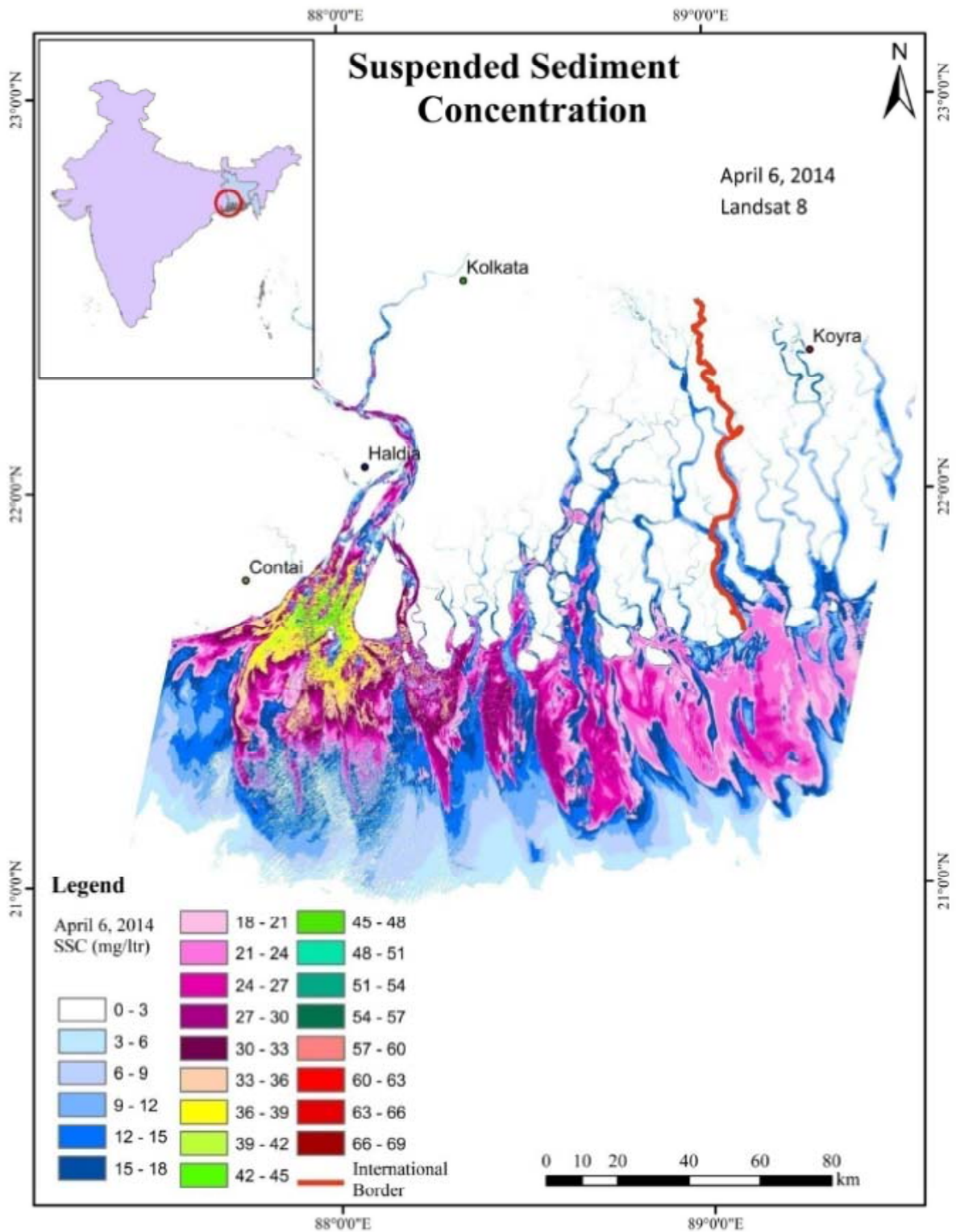


Fig. 10. 2. Suspended sediment concentration (mg/l) in the study area on April 6, 2010.

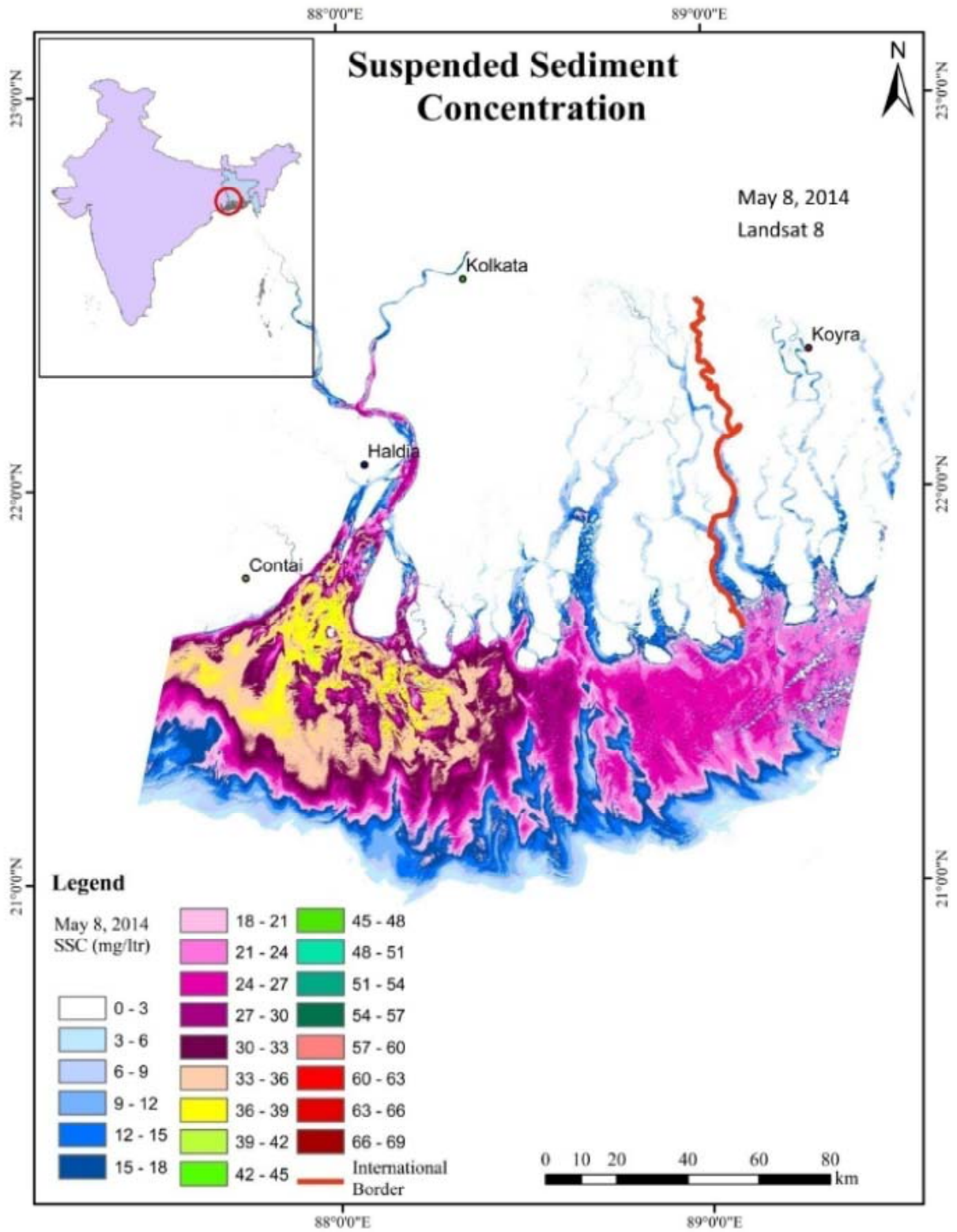


Fig. 10. 3. Suspended sediment concentration (mg/l) in the study area on May 8, 2014.



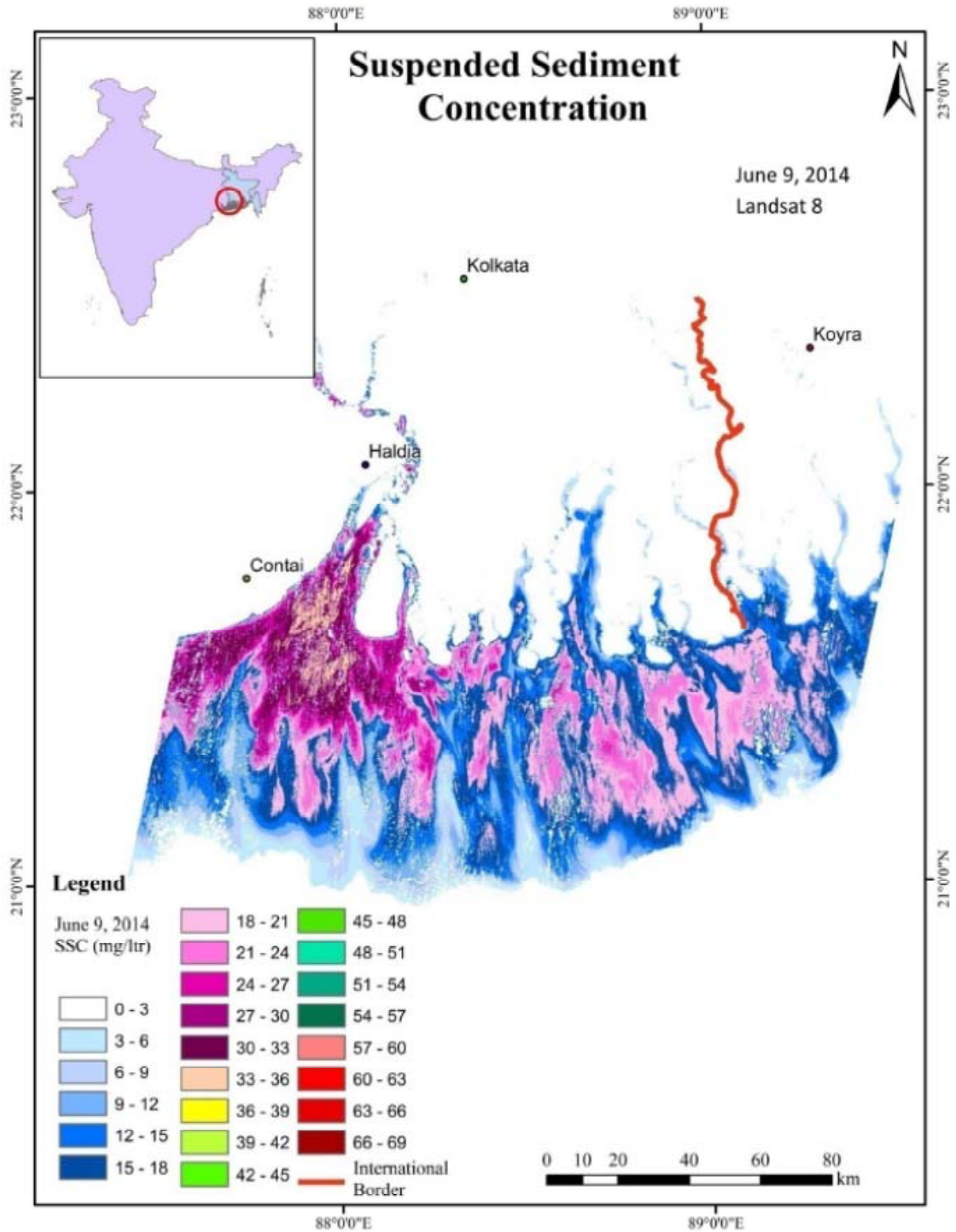


Fig. 10. 4. Suspended sediment concentration (mg/l) in the study area on June 9, 2014.

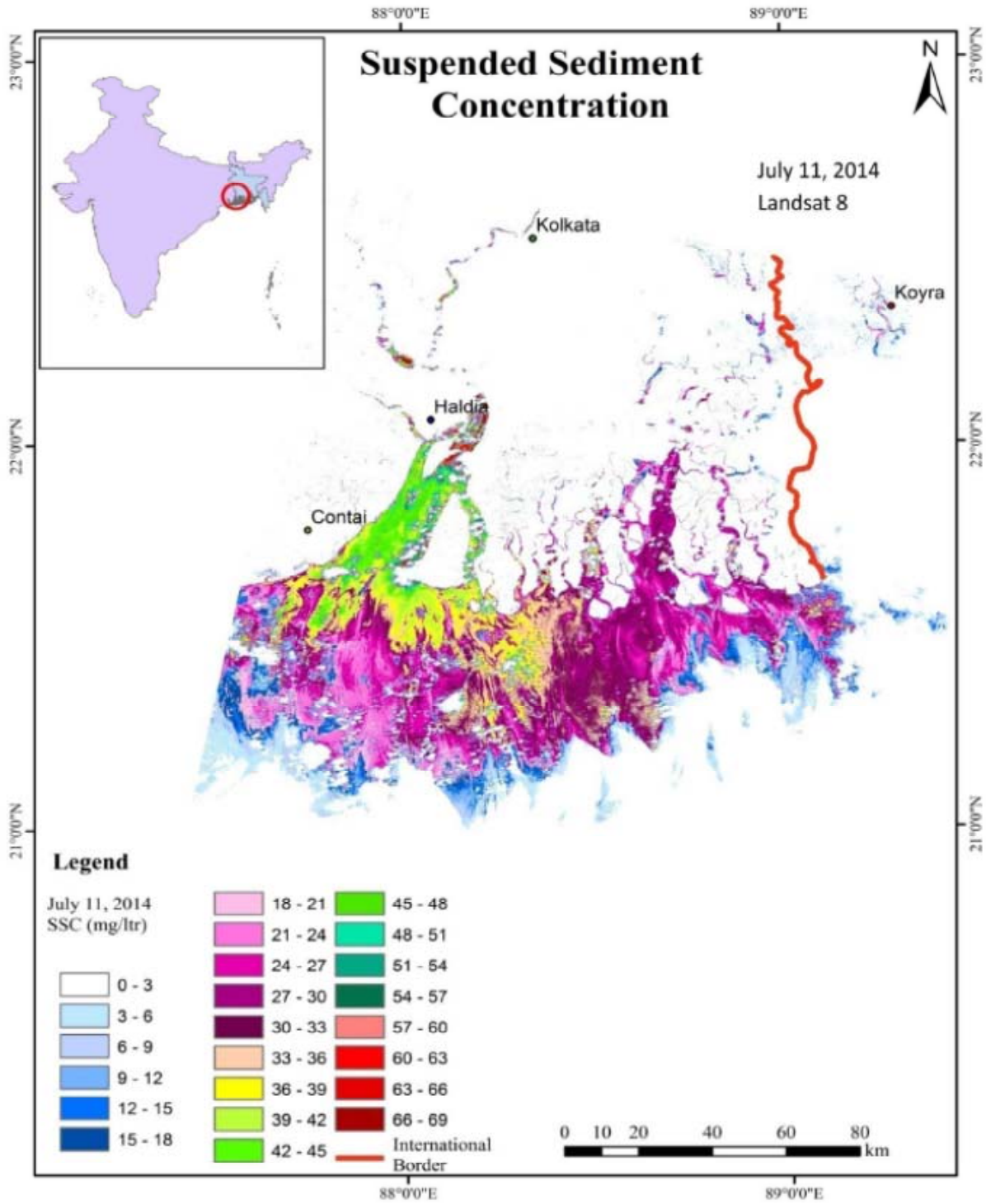


Fig. 11.1. Suspended sediment concentration (mg/l) in the study area on July 11, 2014.

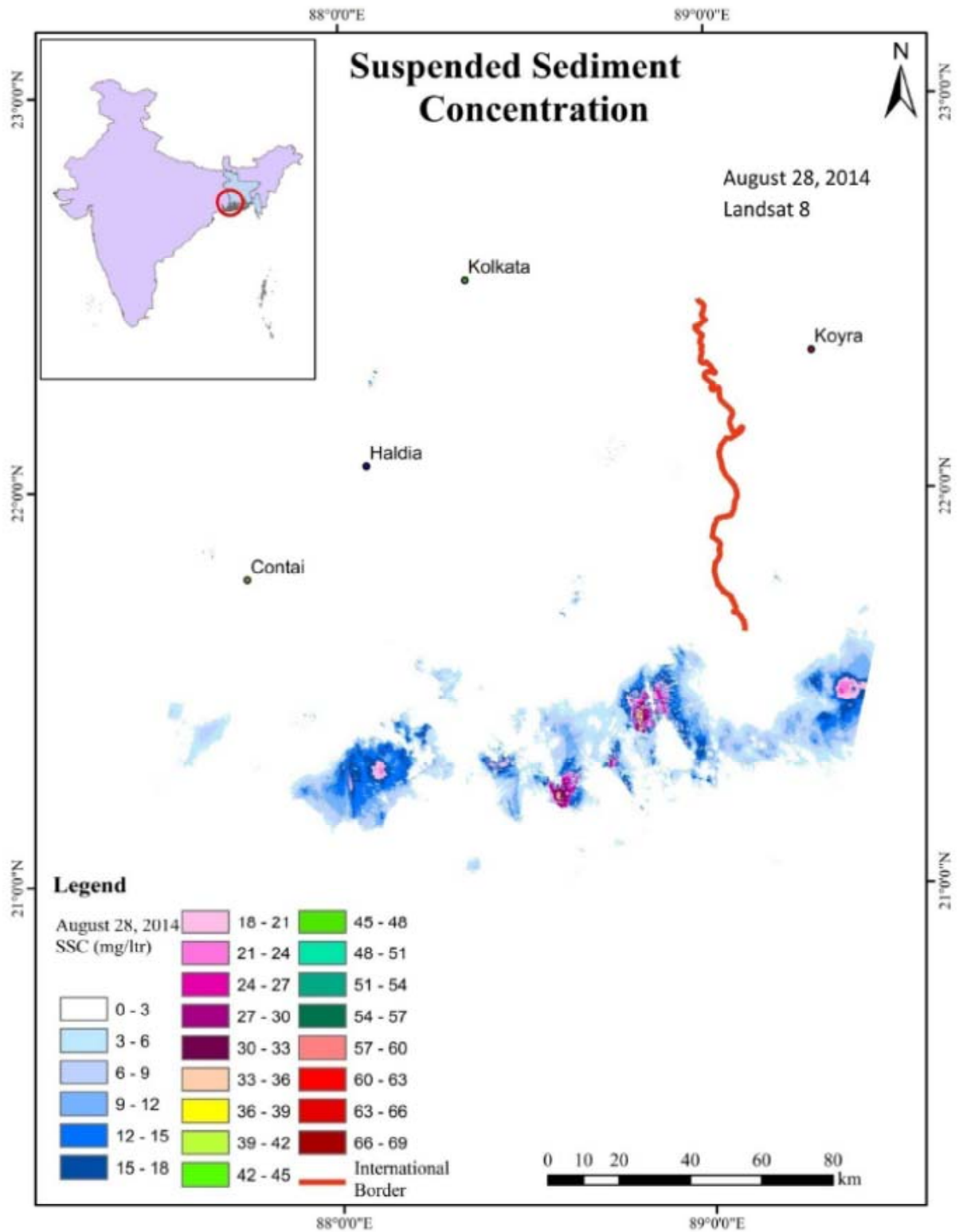


Fig. 11. 2. Suspended sediment concentration (mg/l) in the study area on August 28, 2014.

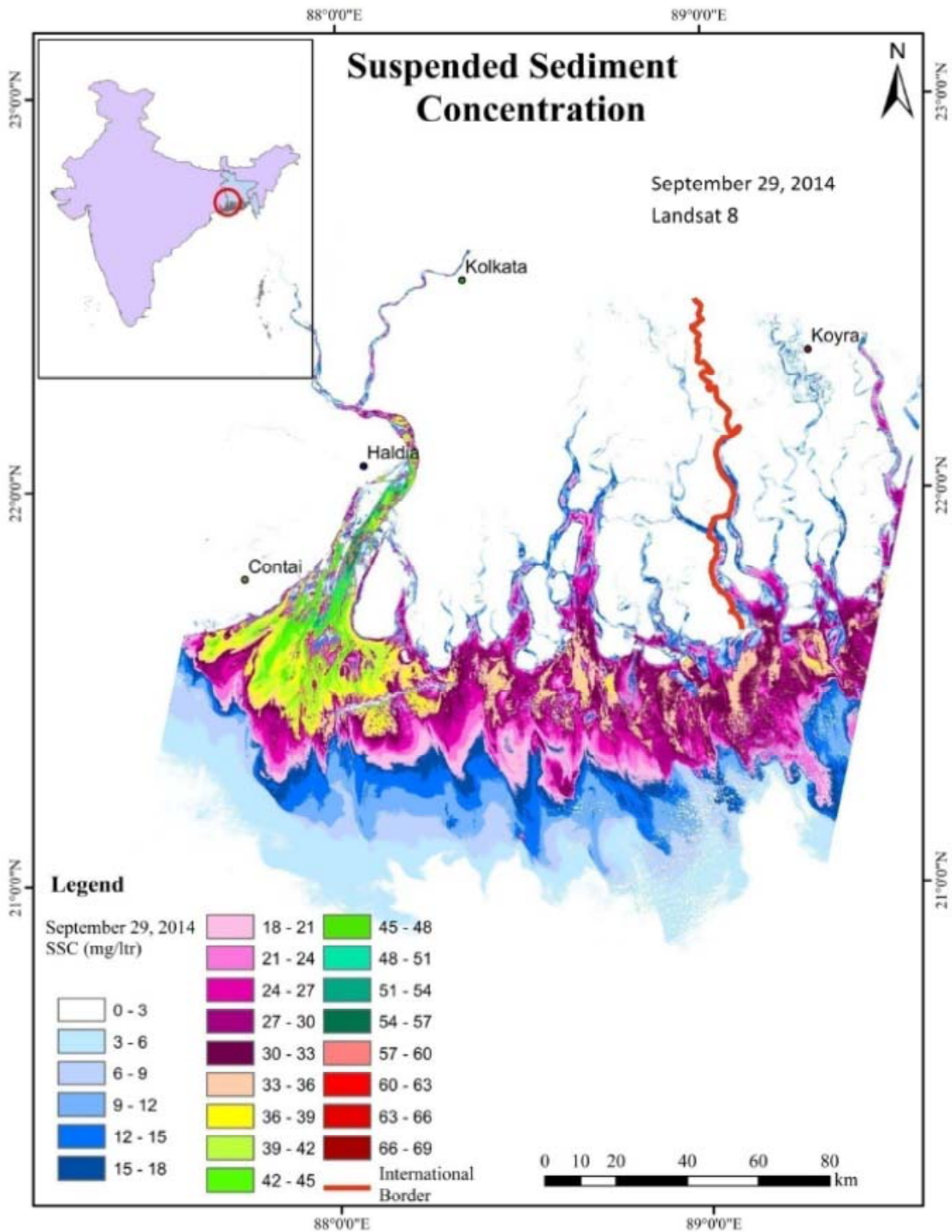


Fig. 11.3. Suspended sediment concentration (mg/l) in the study area on September 29, 2014.



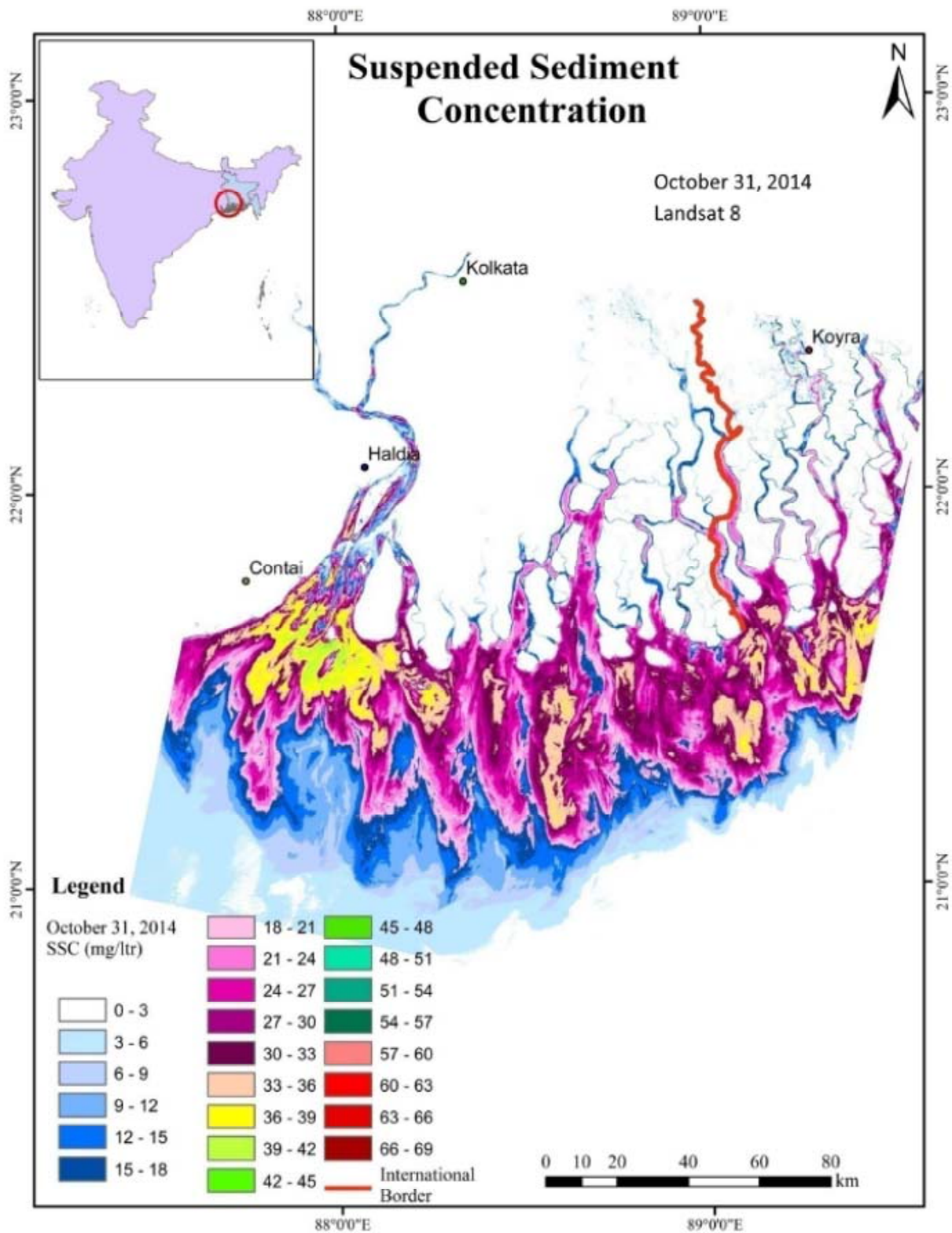


Fig. 11.4. Suspended sediment concentration (mg/l) in the study area on October 31, 2014.

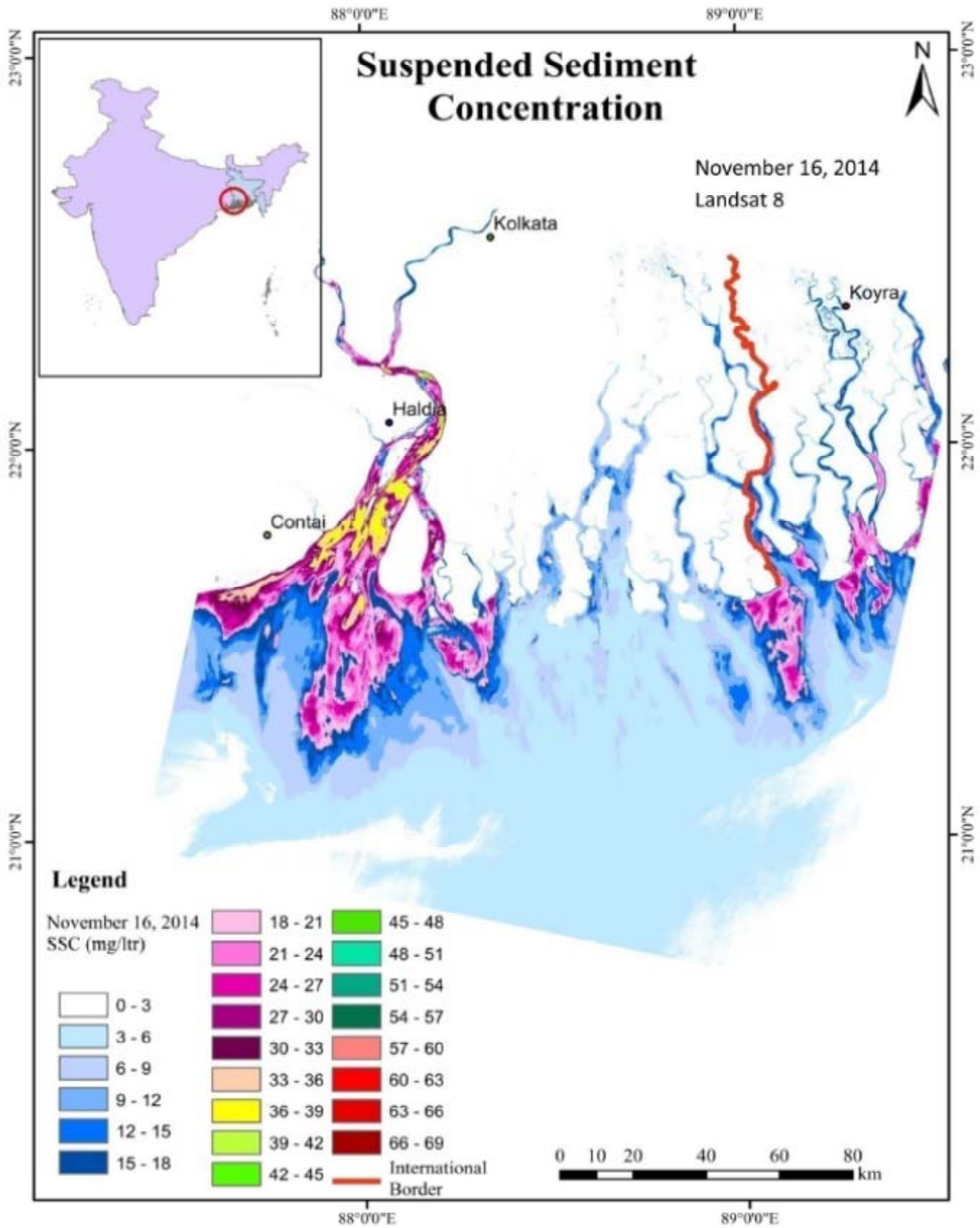


Fig. 12.1. Suspended sediment concentration (mg/l) in the study area on November 16, 2014

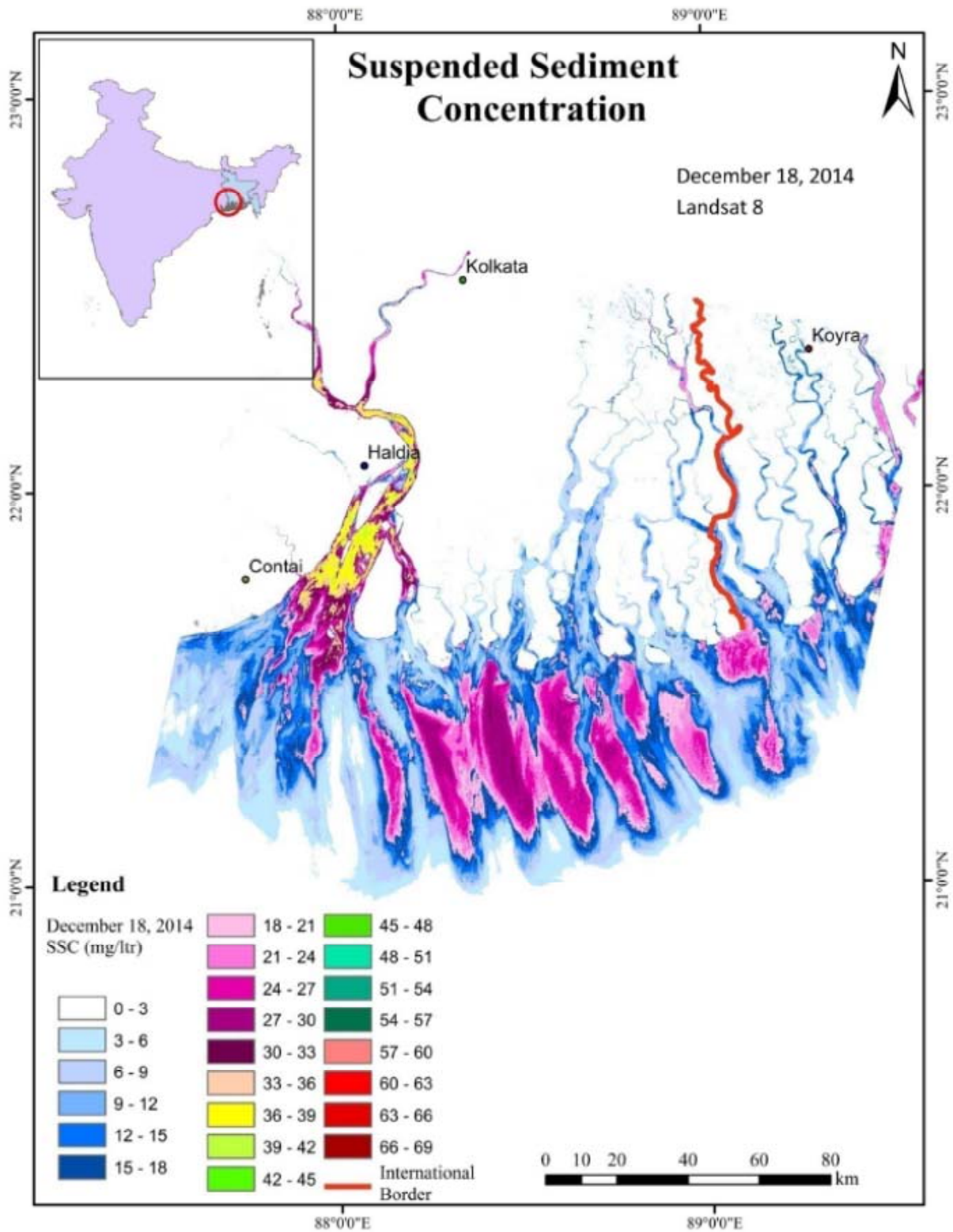


Fig. 12.2. Suspended sediment concentration (mg/l) in the study area on December 31, 2014

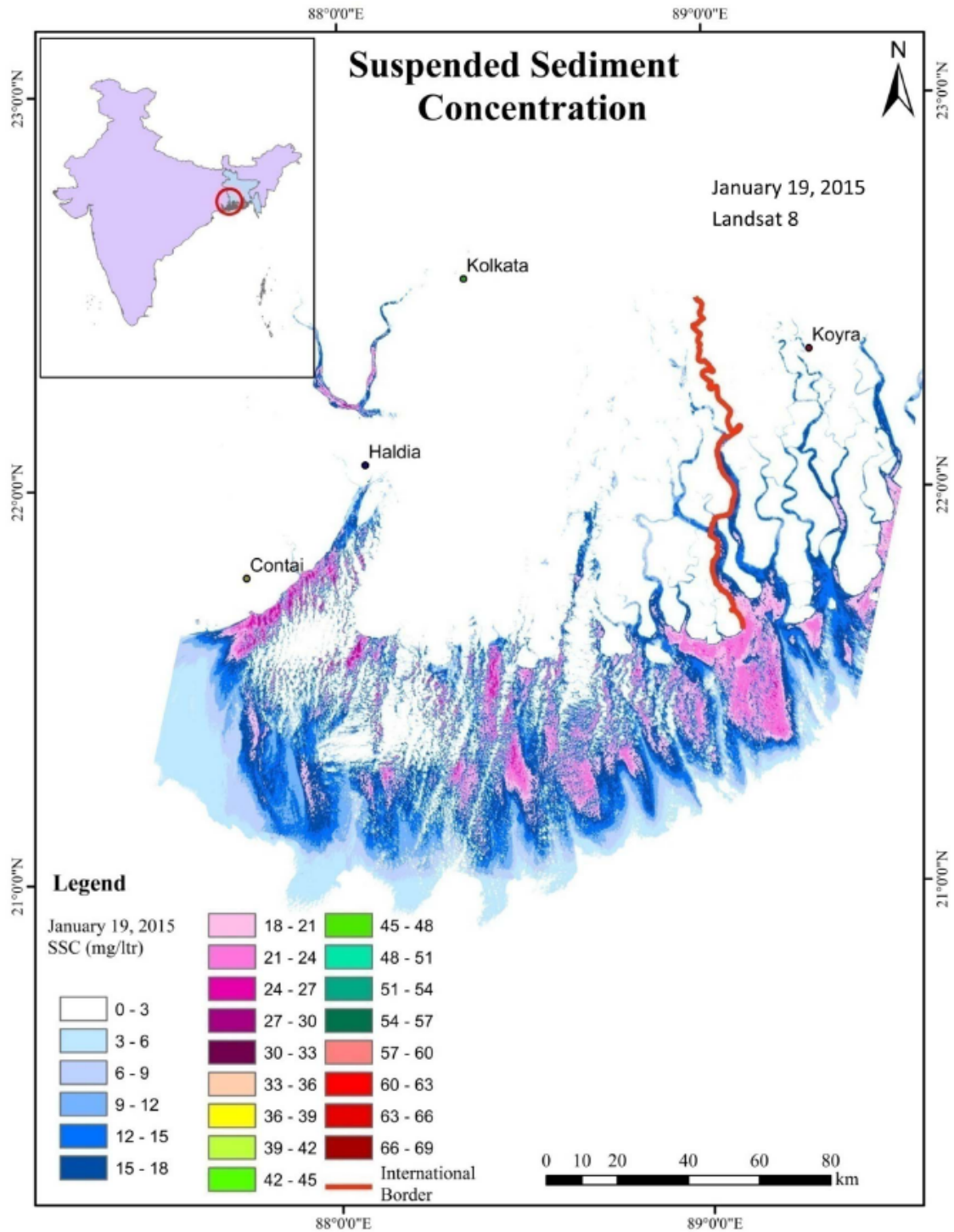


Fig. 12.3. Suspended sediment concentration (mg/l) in the study area on January 19, 2015



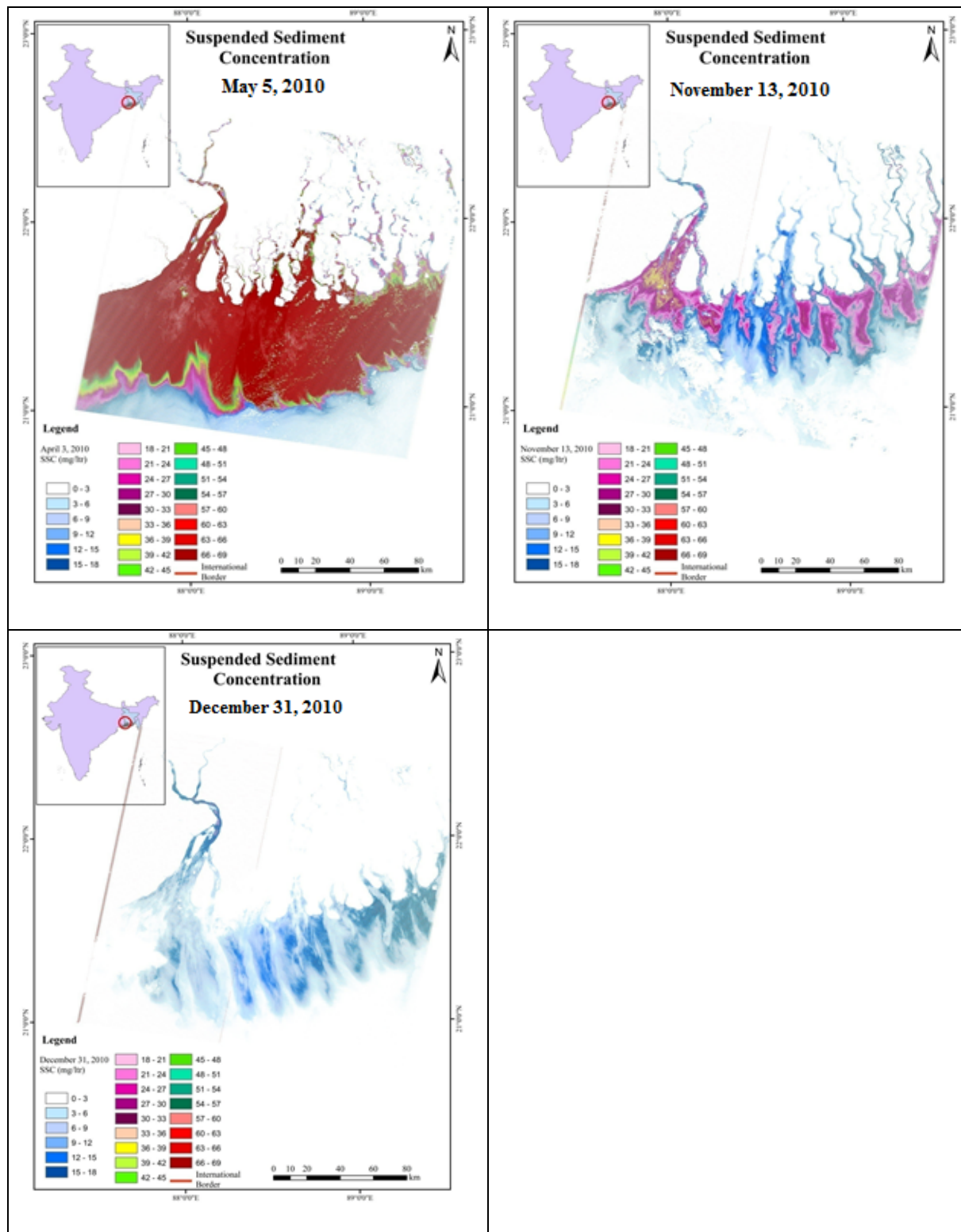


Fig. 9. Suspended sediment concentration for May, November & December months of 2010.

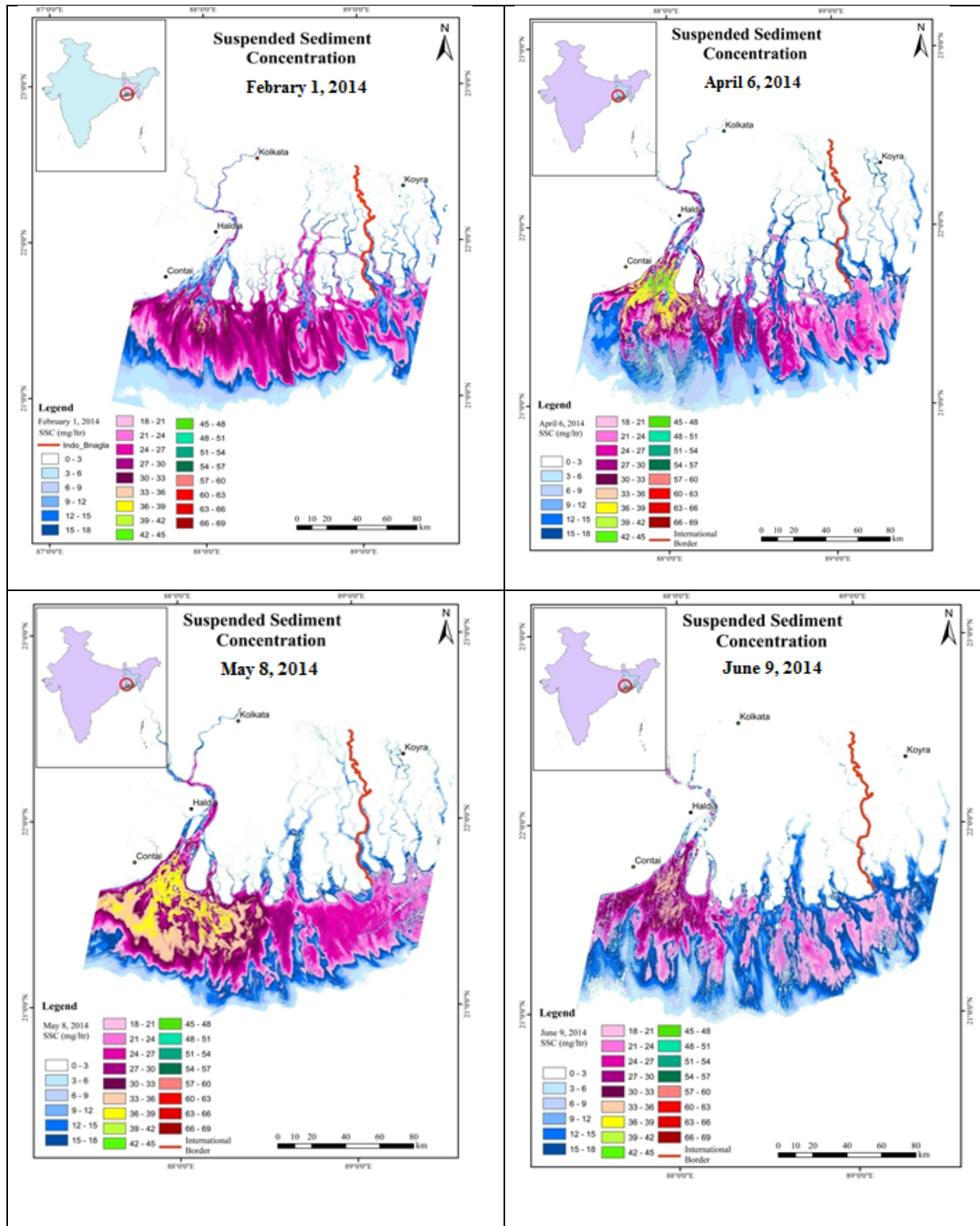


Fig. 10. Suspended sediment concentration for February, April, May, & June months of 2014

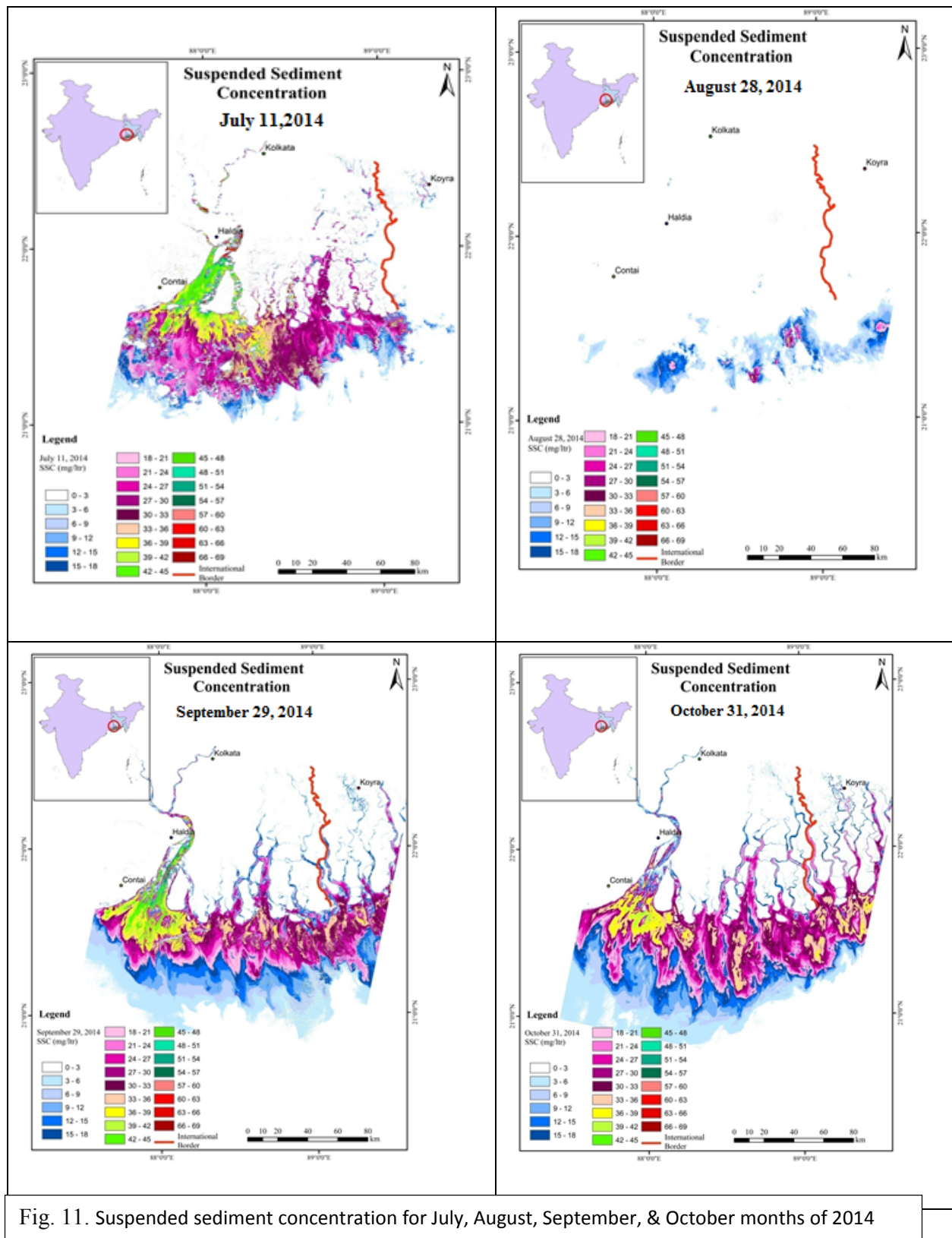


Fig. 11. Suspended sediment concentration for July, August, September, & October months of 2014

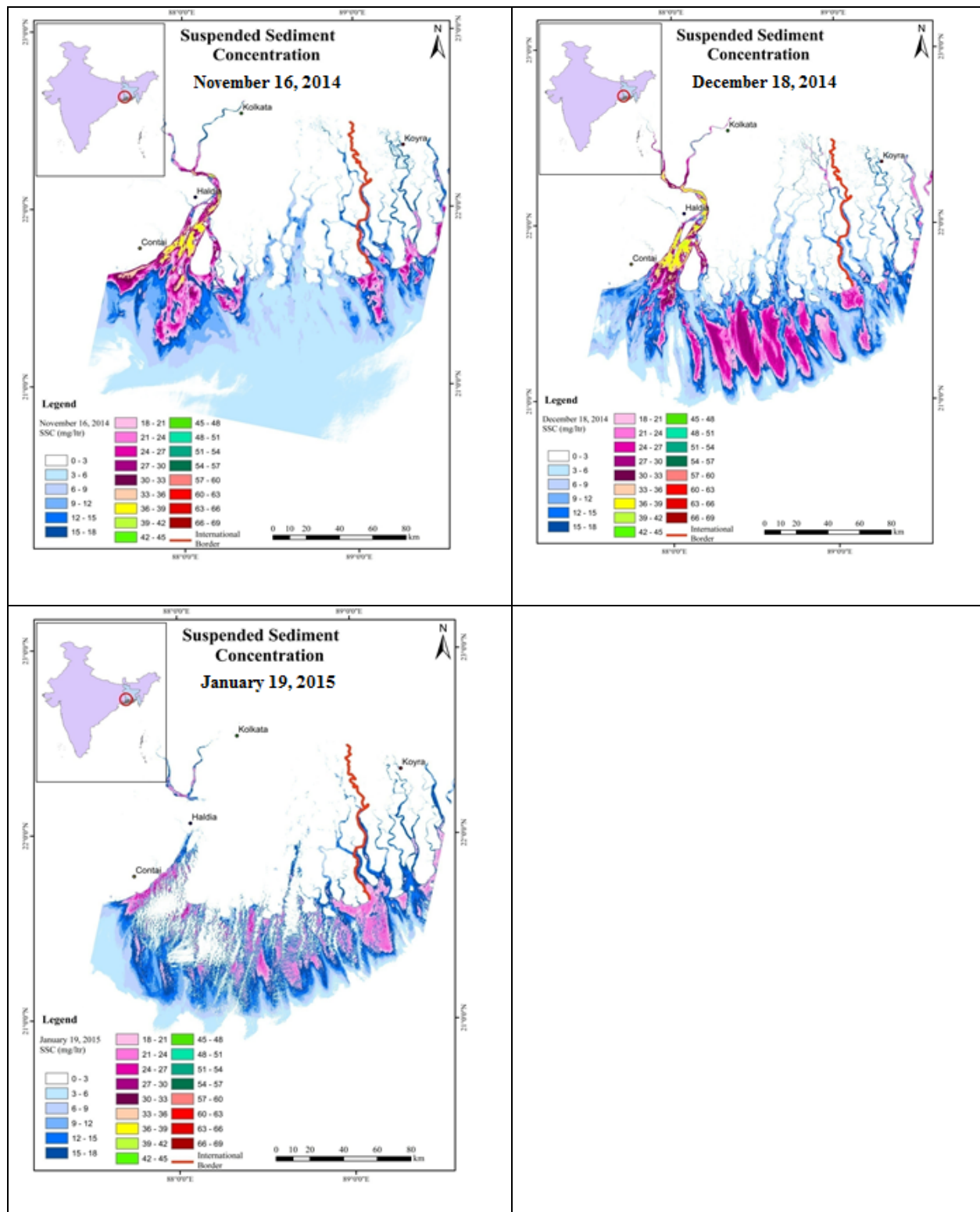


Fig 12. Suspended sediment concentration for November, December 2014 & January months of 2015.